



UNIVERSITY OF LEEDS

This is a repository copy of *Synthesis and characterization of C<sub>2</sub>-symmetric bis(carboxamide) pincer ligands*.

White Rose Research Online URL for this paper:

<https://eprints.whiterose.ac.uk/208745/>

Version: Supplemental Material

---

**Article:**

Razuwika, R. [orcid.org/0000-0001-9831-7759](https://orcid.org/0000-0001-9831-7759) and Munro, O.Q. [orcid.org/0000-0001-8979-6321](https://orcid.org/0000-0001-8979-6321) (2024) *Synthesis and characterization of C<sub>2</sub>-symmetric bis(carboxamide) pincer ligands*. *New Journal of Chemistry*. ISSN 1144-0546

<https://doi.org/10.1039/d3nj05502g>

---

© The Royal Society of Chemistry and the Centre National de la Recherche Scientifique 2024. This is an author produced version of an article published in *New Journal of Chemistry*. Uploaded in accordance with the publisher's self-archiving policy.

**Reuse**

Items deposited in White Rose Research Online are protected by copyright, with all rights reserved unless indicated otherwise. They may be downloaded and/or printed for private study, or other acts as permitted by national copyright laws. The publisher or other rights holders may allow further reproduction and re-use of the full text version. This is indicated by the licence information on the White Rose Research Online record for the item.

**Takedown**

If you consider content in White Rose Research Online to be in breach of UK law, please notify us by emailing [eprints@whiterose.ac.uk](mailto:eprints@whiterose.ac.uk) including the URL of the record and the reason for the withdrawal request.



[eprints@whiterose.ac.uk](mailto:eprints@whiterose.ac.uk)  
<https://eprints.whiterose.ac.uk/>

## Supporting Information:

# Synthesis and Characterization of C<sub>2</sub> Symmetry Bis(Carboxamide) Pincer Ligands

Rufaro Razuwika<sup>\*,a</sup> and Orde Q. Munro<sup>a,b</sup>

<sup>a</sup> Molecular Sciences Institute, School of Chemistry, University of the Witwatersrand, PO WITS 2050, Johannesburg, South Africa

<sup>b</sup> School of Chemistry, University of Leeds, Woodhouse Road, Leeds, LS2 9JT, UK

Email: [razuwika@gmail.com](mailto:razuwika@gmail.com)

Email: [o.munro@leeds.ac.uk](mailto:o.munro@leeds.ac.uk)

---

## Contents

IR instrumentation and spectra.....	4
<b>Figure S1.</b> IR spectra for a powder sample (blue) and from DFT calculated data in a vacuum (red) of <b>1a</b> .....	4
<b>Figure S2.</b> IR spectra for a powder sample (blue) and from DFT calculated data in a vacuum (red) of <b>1b</b> .....	5
<b>Figure S3.</b> IR spectra for a powder sample (blue) and from DFT calculated data in a vacuum (red) of <b>1c</b> .....	6
<b>Figure S4.</b> IR spectra for a powder sample (blue) and from DFT calculated data in a vacuum (red) of <b>1d</b> .....	7
<b>Figure S5.</b> IR spectra for a powder sample (blue) and from DFT calculated data in a vacuum (red) of <b>1e</b> .....	8
<b>Figure S6.</b> IR spectra for a powder sample (blue) and from DFT calculated data in a vacuum (red) of <b>1f</b> .....	9
NMR spectroscopy .....	10
<b>Figure S7.</b> <sup>1</sup> H (a) and <sup>13</sup> C APT (Attached-Proton-Test) (b) NMR spectra of <b>1a</b> in DMSO- <i>d</i> <sub>6</sub> .....	10
<b>Figure S8.</b> <sup>1</sup> H (a) and <sup>13</sup> C APT (b) NMR spectra of <b>1b</b> in DMSO- <i>d</i> <sub>6</sub> .....	11
<b>Figure S9.</b> <sup>1</sup> H (a) and <sup>13</sup> C APT (b) NMR spectra of <b>1c</b> in DMSO- <i>d</i> <sub>6</sub> .....	12
<b>Figure S10.</b> <sup>1</sup> H (a) and <sup>13</sup> C APT (b) NMR spectra of <b>1d</b> in DMSO- <i>d</i> <sub>6</sub> .....	13
<b>Figure S11.</b> <sup>1</sup> H (a) and <sup>13</sup> C APT (b) NMR spectra of <b>1e</b> in MeCN- <i>d</i> <sub>3</sub> .....	14
<b>Figure S12.</b> <sup>1</sup> H (a) and <sup>13</sup> C (b) NMR spectra of <b>1f</b> in DMSO- <i>d</i> <sub>6</sub> .....	15
UV-vis spectroscopy.....	16
<b>Figure S13.</b> (a) Experimental and (b) DFT-calculated electronic absorption spectra of <b>1a</b> in DMSO. The absorption maxima are indicated for the experimental spectrum at 277, 309 and 323 nm. The absorption envelope for the DFT-calculated spectrum is plotted with a band width of 2200 cm <sup>-1</sup> (full width at half maximum intensity, FWHM). (c) Absorption spectra at a concentration range between 16 and 157 μM, and (d) Linear Beer-Lambert plot (Beer-Lambert's Law), to calculate the extinction coefficients at at the λ <sub>max</sub> .....	16

<b>Figure S14.</b> (a) Experimental and (b) DFT-calculated electronic absorption spectra of <b>1b</b> in DMSO. The absorption maxima are indicated for the experimental spectrum at 275, 312, 324 and 338 nm. The absorption envelope for the DFT-calculated spectrum is plotted with a bandwidth of 2200 cm <sup>-1</sup> (full width at half maximum intensity, FWHM). (c) Absorption spectra at a concentration range between 4 and 75 μM, and (d) Linear Beer-Lambert plot (Beer-Lambert's Law), to calculate the extinction coefficients at at the λ <sub>max</sub> .....	17
<b>Figure S15.</b> (a) Experimental and (b) DFT-calculated electronic absorption spectra of <b>1c</b> in DMSO. The absorption maxima are indicated for the experimental spectrum at 326 nm. The absorption envelope for the DFT-calculated spectrum is plotted with a bandwidth of 2200 cm <sup>-1</sup> (full width at half maximum intensity, FWHM). (c) Absorption spectra at a concentration range between 2 and 25 μM, and (d) Linear Beer-Lambert plot (Beer-Lambert's Law), to calculate the extinction coefficients at at the λ <sub>max</sub> .....	18
<b>Figure S16.</b> (a) Experimental and (b) DFT-calculated electronic absorption spectra of <b>1d</b> in ACN. The absorption maxima are indicated for the experimental spectrum at 199, 223, 285 nm. The absorption envelope for the DFT-calculated spectrum is plotted with a bandwidth of 2200 cm <sup>-1</sup> (full width at half maximum intensity, FWHM). (c) Absorption spectra at a concentration range between 4 and 38 μM, and (d) Linear Beer-Lambert plot (Beer-Lambert's Law), to calculate the extinction coefficients at at the λ <sub>max</sub> .....	19
<b>Figure S17</b> (a) Experimental and (b) DFT-calculated electronic absorption spectra of <b>1e</b> in DMSO. The absorption maxima are indicated for the experimental spectrum at 330 nm. The absorption envelope for the DFT-calculated spectrum is plotted with a bandwidth of 2200 cm <sup>-1</sup> (full width at half maximum intensity, FWHM). (c) Absorption spectra at a concentration range between 14 and 136 μM, and (d) Linear Beer-Lambert plot (Beer-Lambert's Law), to calculate the extinction coefficients at at the λ <sub>max</sub> .....	20
<b>Figure S18.</b> (a) Experimental and (b) DFT-calculated electronic absorption spectra of <b>1f</b> in DMSO. The absorption maxima are indicated for the experimental spectrum at 269 and 315 nm. The absorption envelope for the DFT-calculated spectrum is plotted with a bandwidth of 2200 cm <sup>-1</sup> (full width at half maximum intensity, FWHM). (c) Absorption spectra at a concentration range between 4 and 62 μM, and (d) Linear Beer-Lambert plot (Beer-Lambert's Law), to calculate the extinction coefficients at at the λ <sub>max</sub> .....	21
<b>Table 1.</b> Calculated energies for orbital levels involved in electron transition.....	22
<b>Table 2.</b> Difference in energy between different HOMO and LUMO energy levels in eV.....	22
Mass spectroscopy.....	23
<b>Figure S19.</b> ESI-MS spectrum of <b>1a</b> for C <sub>23</sub> H <sub>18</sub> N <sub>5</sub> O <sub>2</sub> [M+H] <sup>+</sup> = 420.416. The solid sample was dissolved in ACN (1 % DMSO) with 0.1% formic acid (v/v) and the spectrum was recorded in positive ESI mode. ....	23
<b>Figure S20.</b> ESI-MS spectrum of <b>1b</b> for C <sub>23</sub> H <sub>18</sub> N <sub>5</sub> O <sub>2</sub> [M+H] <sup>+</sup> = 420.146. The solid sample was dissolved in ACN (1 % DMSO) with 0.1% formic acid (v/v) and the spectrum was recorded in positive ESI mode. ....	23
<b>Figure S21.</b> ESI-MS spectrum of <b>1c</b> for C <sub>23</sub> H <sub>18</sub> N <sub>5</sub> O <sub>2</sub> [M+H] <sup>+</sup> = 420.146. The solid sample was dissolved in ACN (1 % DMSO) with 0.1% formic acid (v/v) and the spectrum was recorded in positive ESI mode. ....	24
<b>Figure S22.</b> ESI-MS spectrum of <b>1d</b> for C <sub>23</sub> H <sub>18</sub> N <sub>5</sub> O <sub>2</sub> [M+H] <sup>+</sup> = 420.146. The solid sample was dissolved in ACN with 0.1% formic acid (v/v) and the spectrum was recorded in positive ESI mode.....	24
<b>Figure S23.</b> ESI-MS spectrum of <b>1e</b> for C <sub>23</sub> H <sub>18</sub> N <sub>5</sub> O <sub>2</sub> [M+H] <sup>+</sup> = 426.167. The solid sample was dissolved in ACN (1 % DMSO) with 0.1% formic acid (v/v) and the spectrum was recorded in positive ESI mode. ....	25
<b>Figure S24.</b> ESI-MS spectrum of <b>1f</b> for C <sub>23</sub> H <sub>18</sub> N <sub>5</sub> O <sub>2</sub> [M+H] <sup>+</sup> = 522.1773. The solid sample was dissolved in methanol with 0.1% formic acid (v/v) and the spectrum was recorded in positive ESI mode. ....	25
Xray crystallography.....	26
<b>Figure S25.</b> View of a pair of neighboring molecules in the crystal lattice of <b>1b</b> . The non-classical hydrogen bond C22–H22...N4 (2.491(7) Å) tips the quinoline ring out of the mean plane encompassing the central pyridine ring of the pincer, with the dihedral angle C19–N1–C2–C1 measuring 162.87(5)°. The dihedral angle for the second quinoline group (C25–N3–C11–C10, 176.31(5)°) is almost coplanar with the amide group and central pyridine ring.....	26
<b>Figure S26.</b> Space filling views of the hydrogen-bonded C <sub>i</sub> symmetry dimer of structure <b>1a</b> . The diagram at the left is a view from above the dimer perpendicular to the plane of the pincer's central pyridine ring, while the	

diagram at the right is the same view rotated counterclockwise through  $90^\circ$  to highlight the out-of-plane arrangement of the two isoquinoline rings. The conformation of each monomer in the crystalline solid state is markedly different from the lowest-energy conformer in the gas phase (DFT simulation), which highlights the impact of crystal packing and dimer formation on the observed conformation..... 26

**Figure S27.** View depicting the short nonbonded interactions (blue stippled bonds) between the lower quinoline ring of **1c** and neighboring molecule heteroaromatic rings (contact distances are given in Å). The highlighted contacts constitute C–H... $\pi$  type hydrogen bonding interactions which planarise the amide group (N1) and quinoline substituent by neatly sandwiching the substituent group. The quinoline ring appended to the second amide nitrogen atom (N5) lacks short contacts involving its aryl ring carbon atoms and thus has a more canted dihedral angle relative to the plane of the central pyridine ring of the pincer..... 27

IR instrumentation and spectra

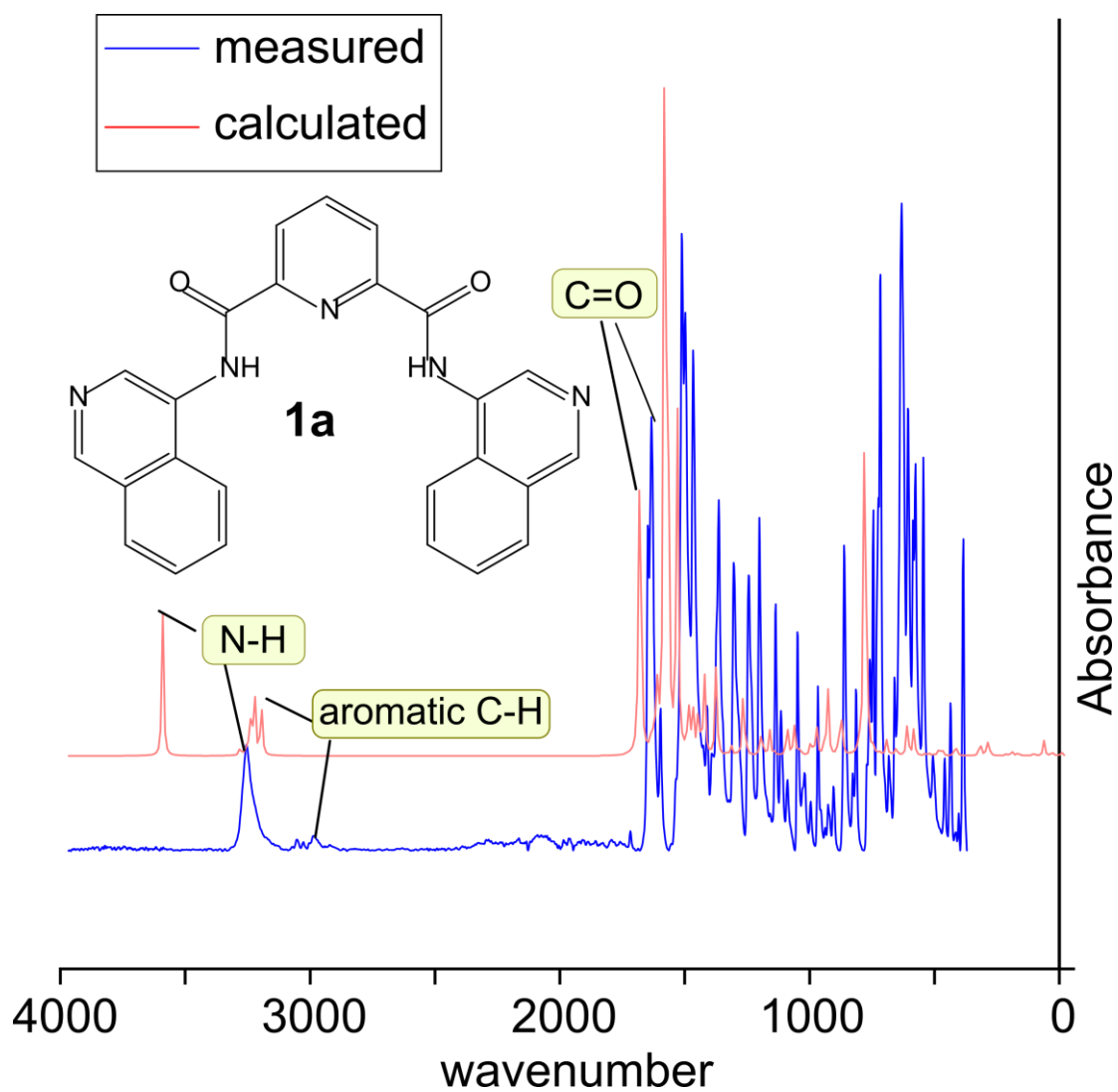


Figure S1. IR spectra for a powder sample (blue) and from DFT calculated data in a vacuum (red) of **1a**.

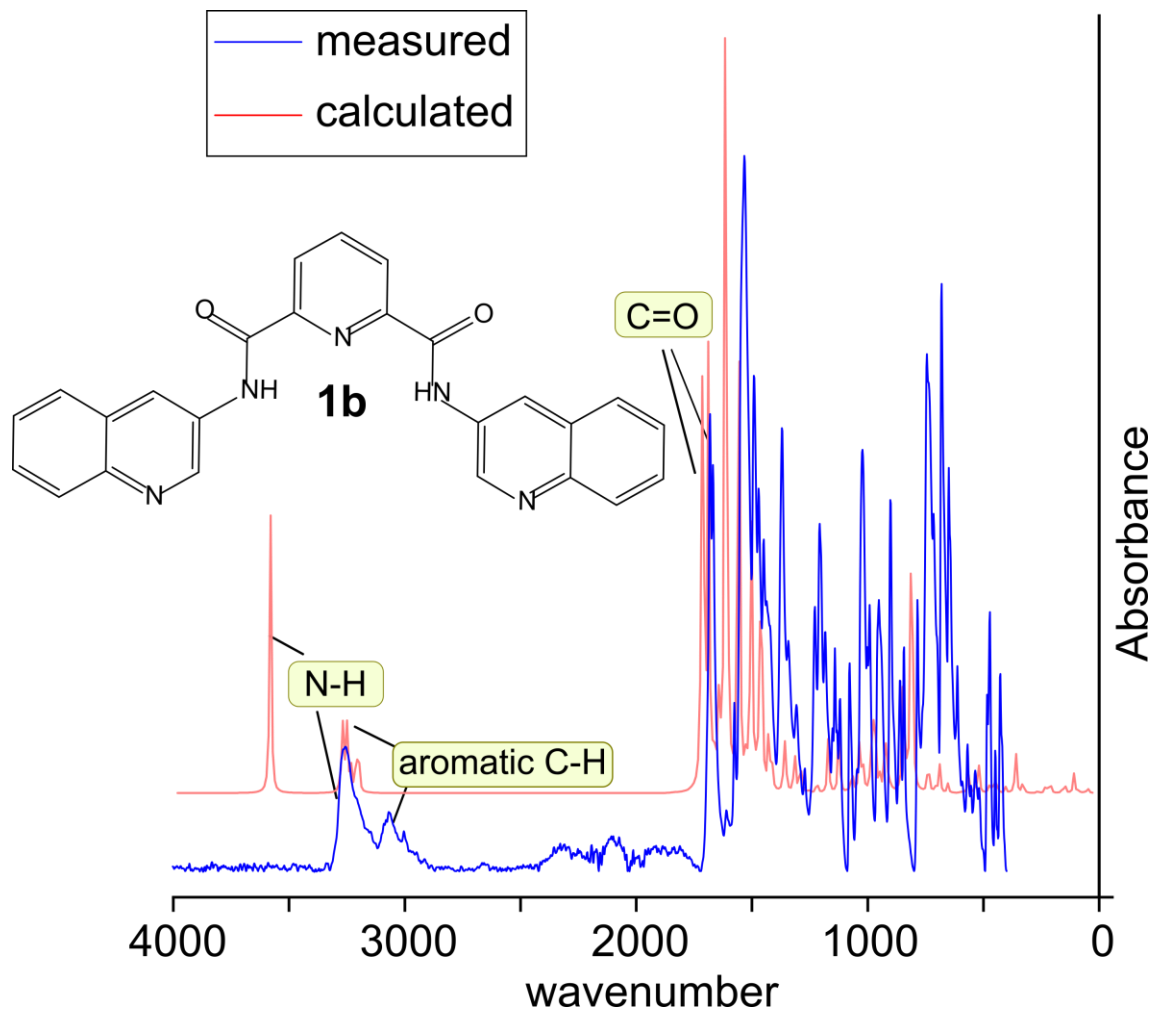


Figure S2. IR spectra for a powder sample (blue) and from DFT calculated data in a vacuum (red) of **1b**.

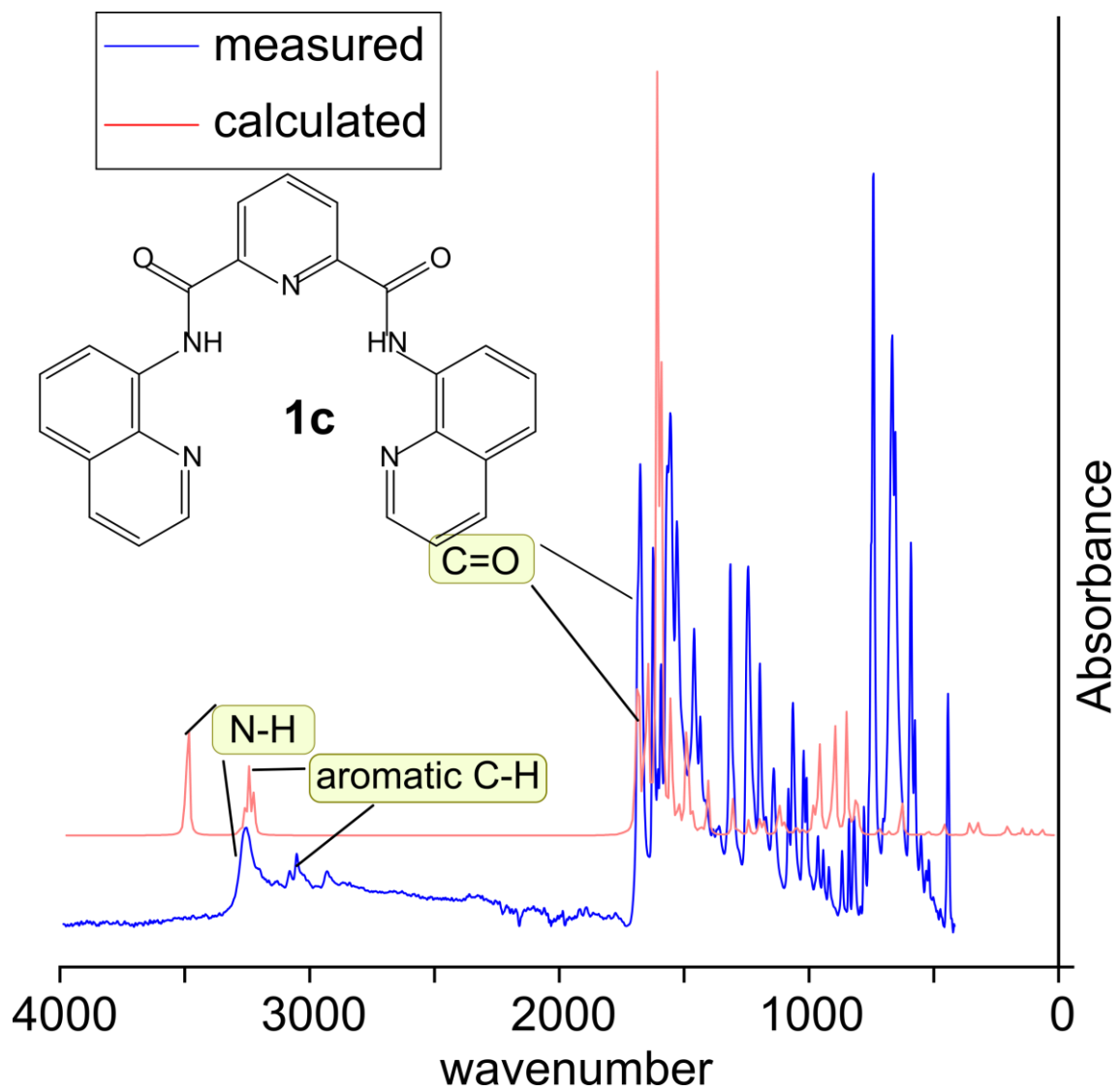


Figure S3. IR spectra for a powder sample (blue) and from DFT calculated data in a vacuum (red) of **1c**.

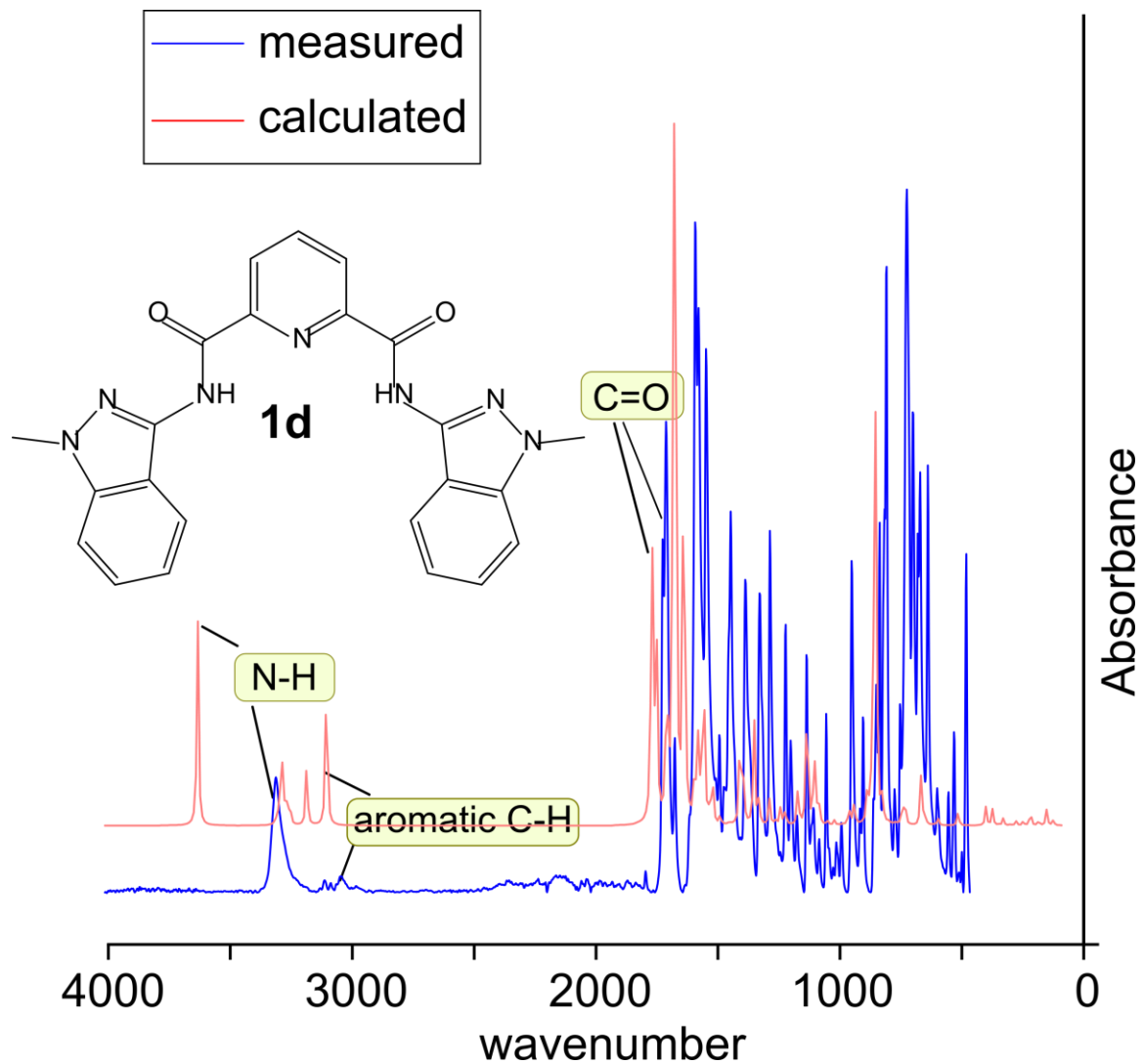


Figure S4. IR spectra for a powder sample (blue) and from DFT calculated data in a vacuum (red) of **1d**.

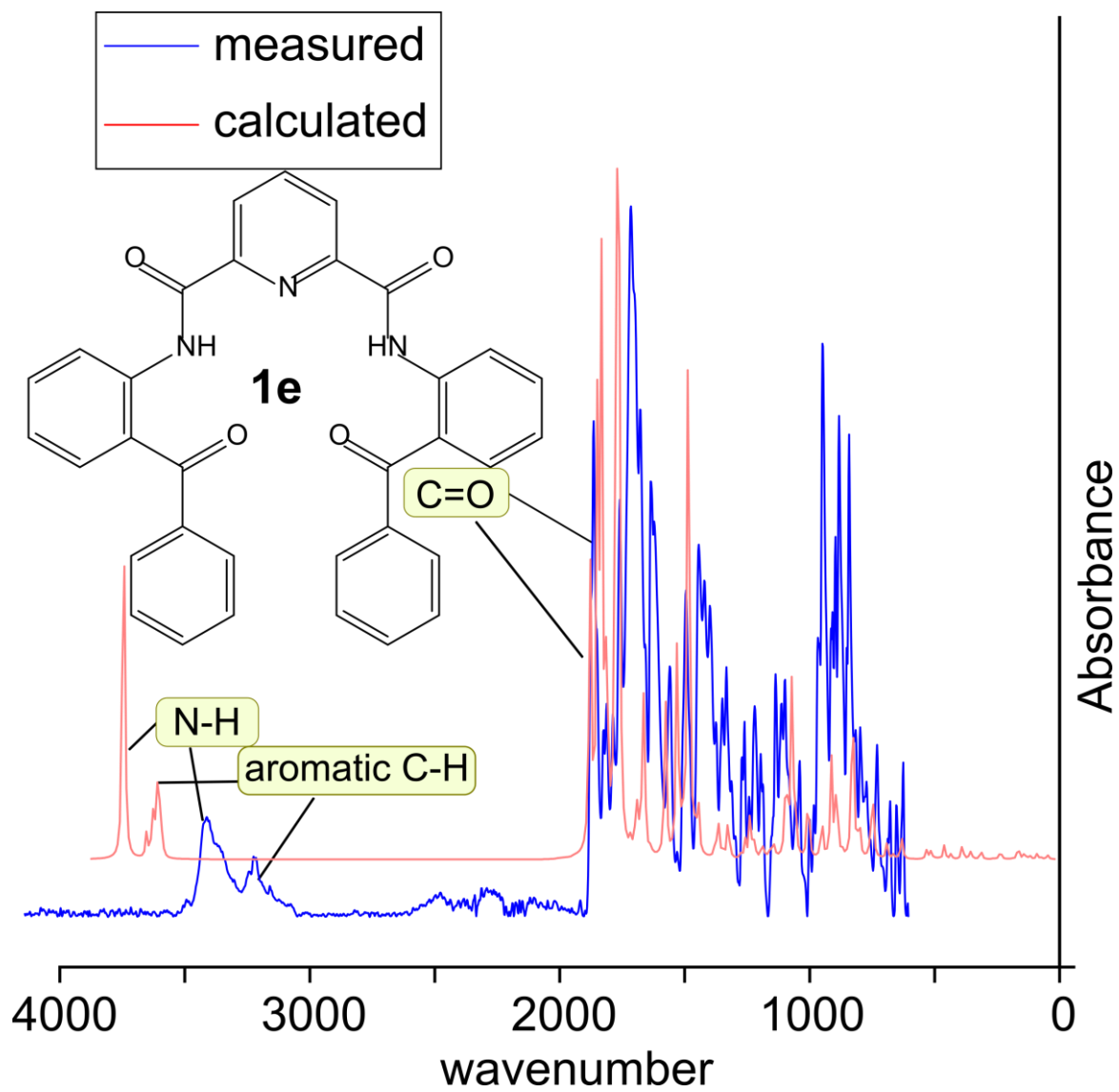


Figure S5. IR spectra for a powder sample (blue) and from DFT calculated data in a vacuum (red) of **1e**.

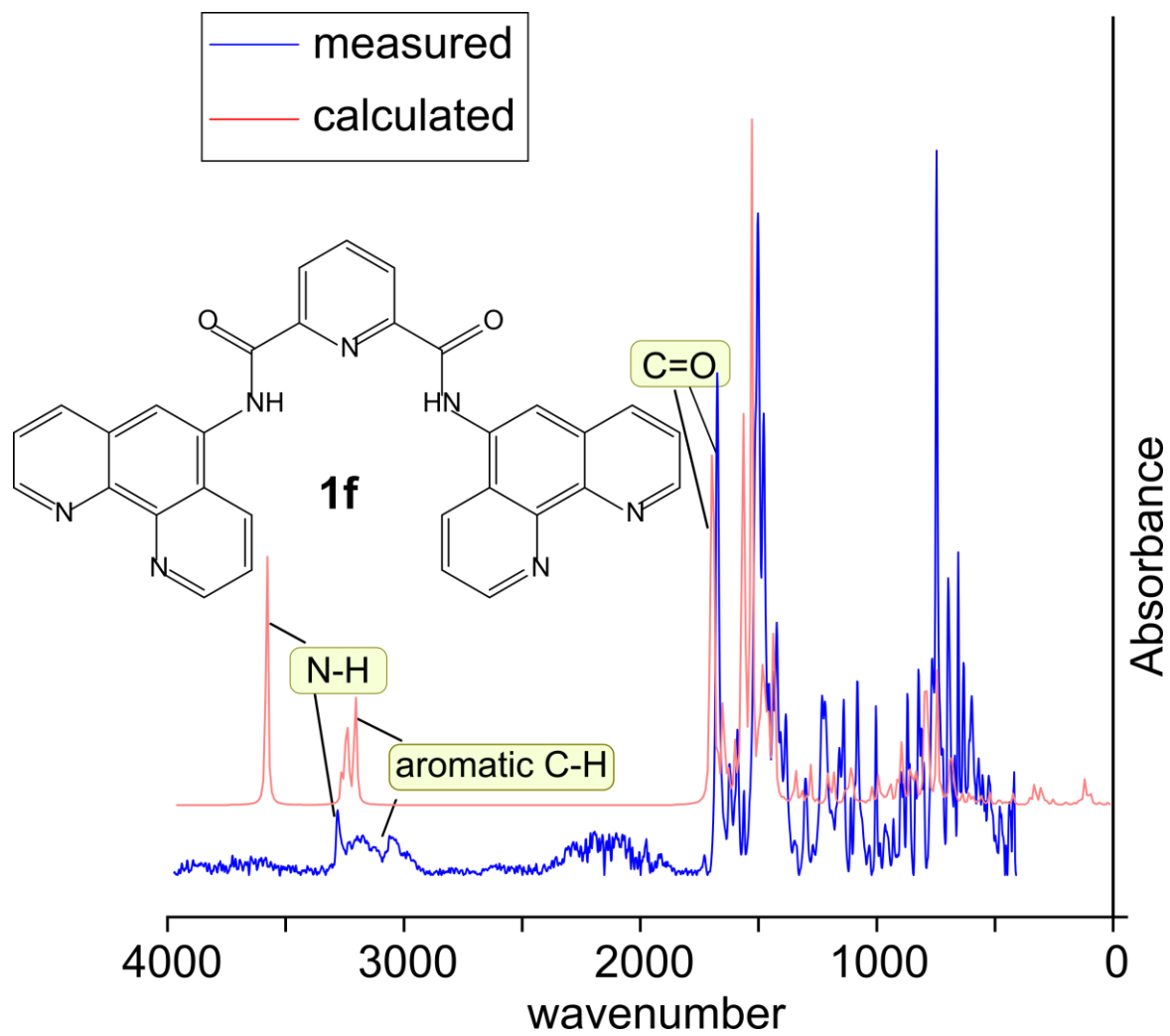
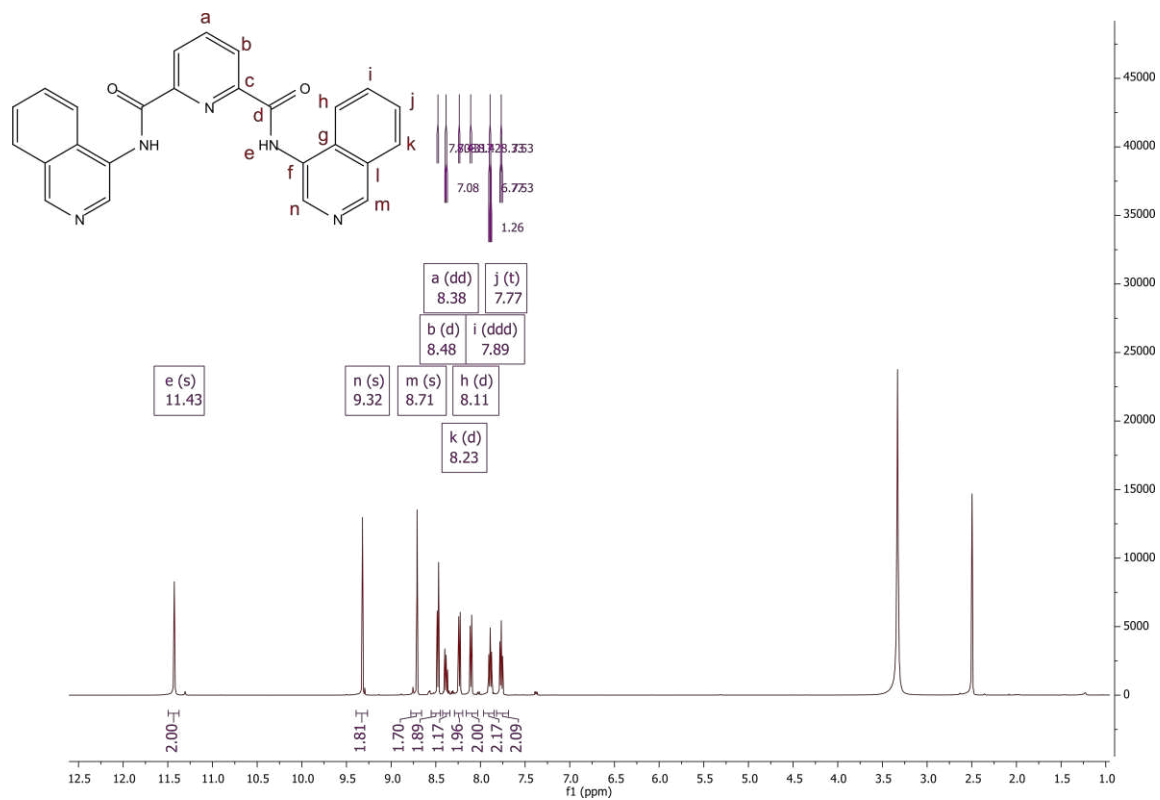


Figure S6. IR spectra for a powder sample (blue) and from DFT calculated data in a vacuum (red) of **1f**.

# NMR spectroscopy

a)



b)

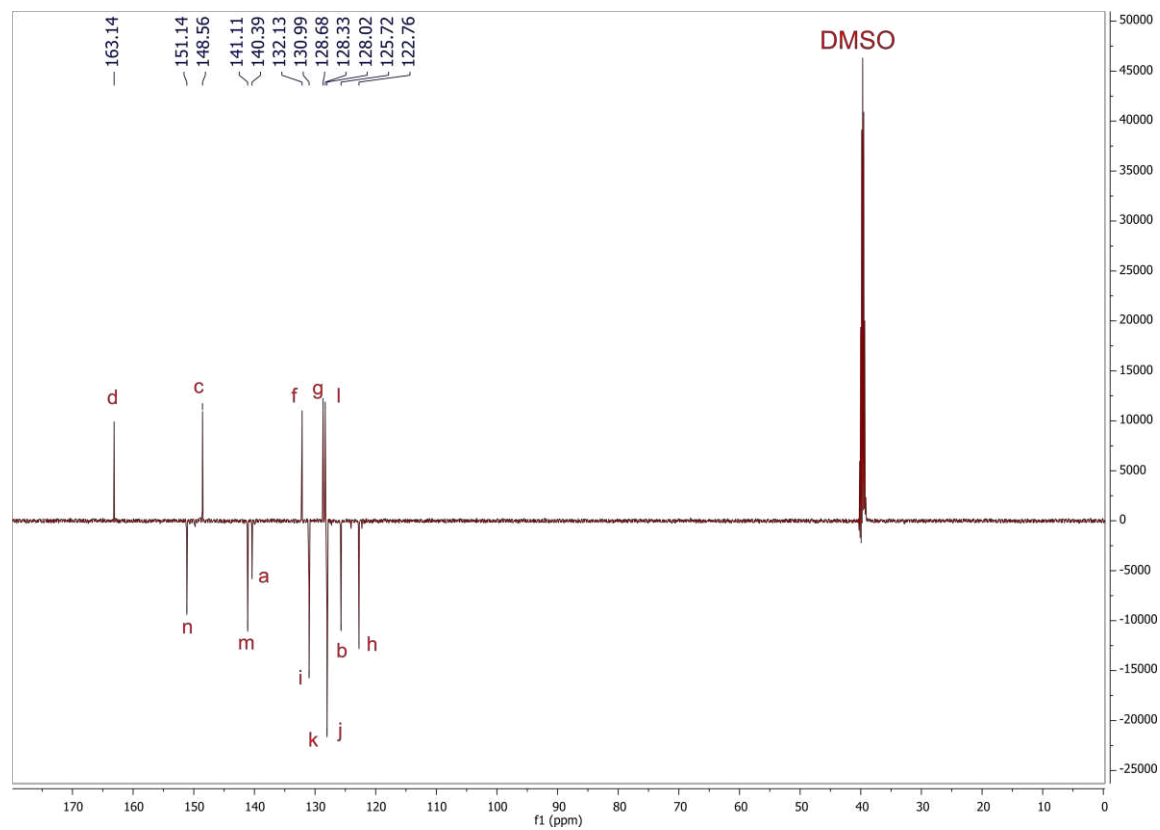
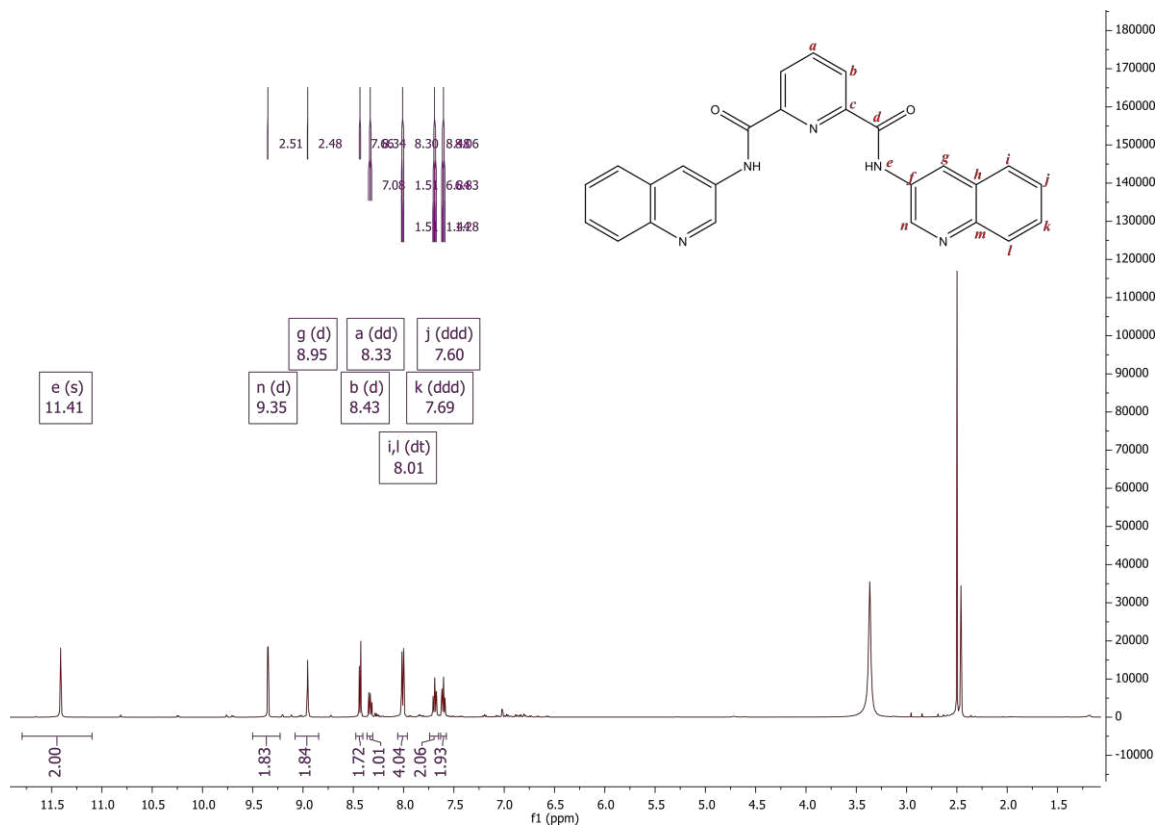


Figure S7.  $^1\text{H}$  (a) and  $^{13}\text{C}$  APT (Attached-Proton-Test) (b) NMR spectra of **1a** in  $\text{DMSO-}d_6$ .

a)



b)

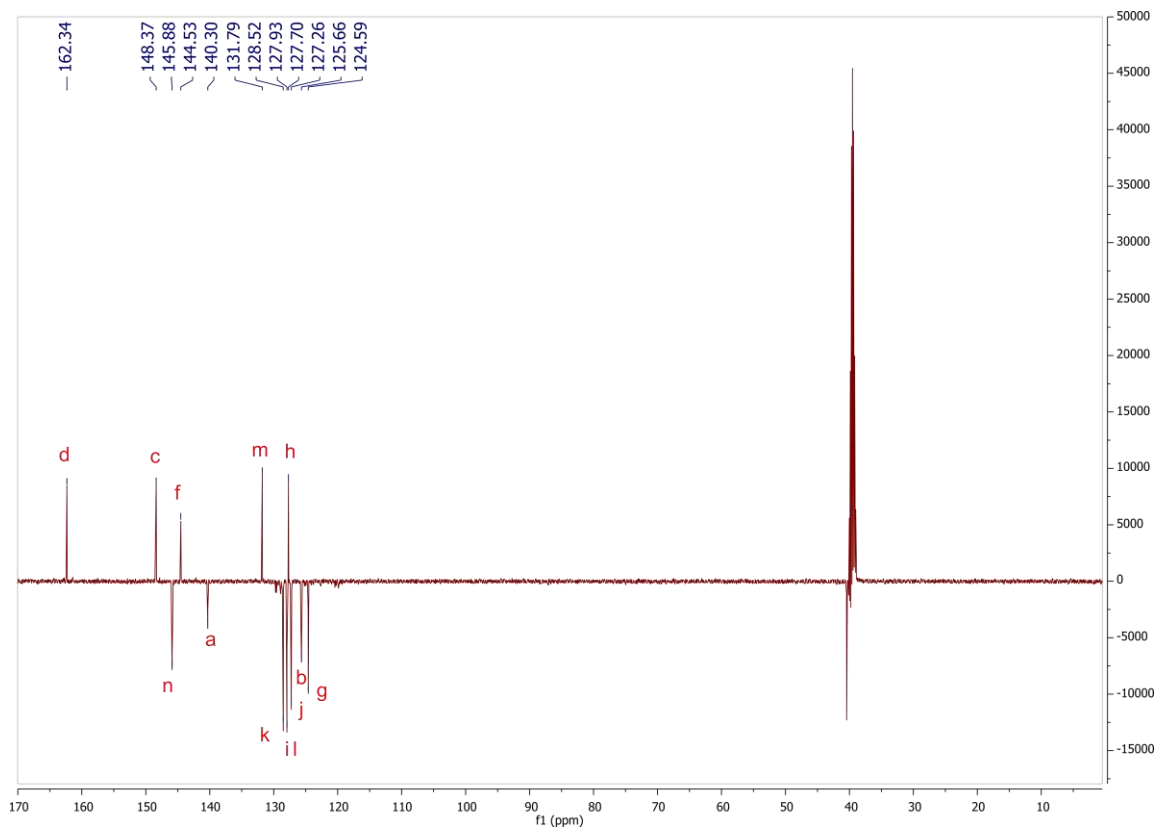
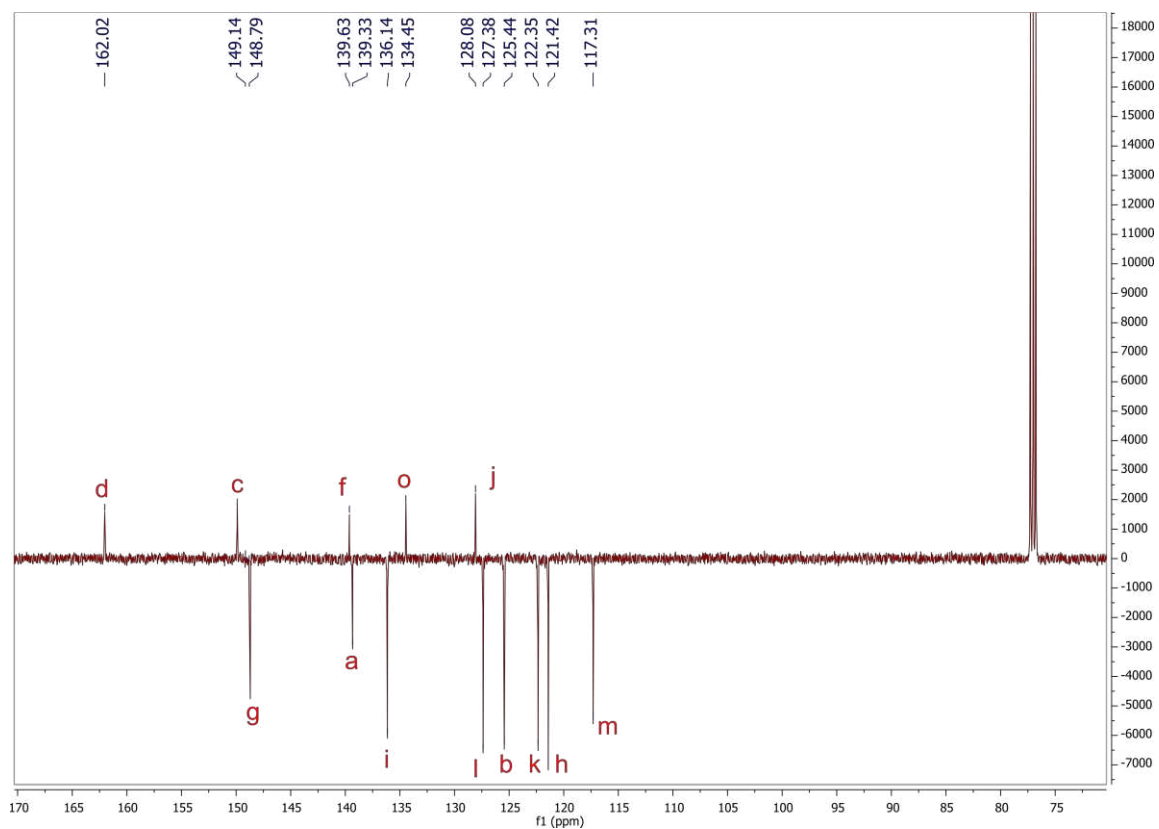


Figure S8.  $^1\text{H}$  (a) and  $^{13}\text{C}$  APT (b) NMR spectra of **1b** in  $\text{DMSO}-d_6$ .

a)



b)

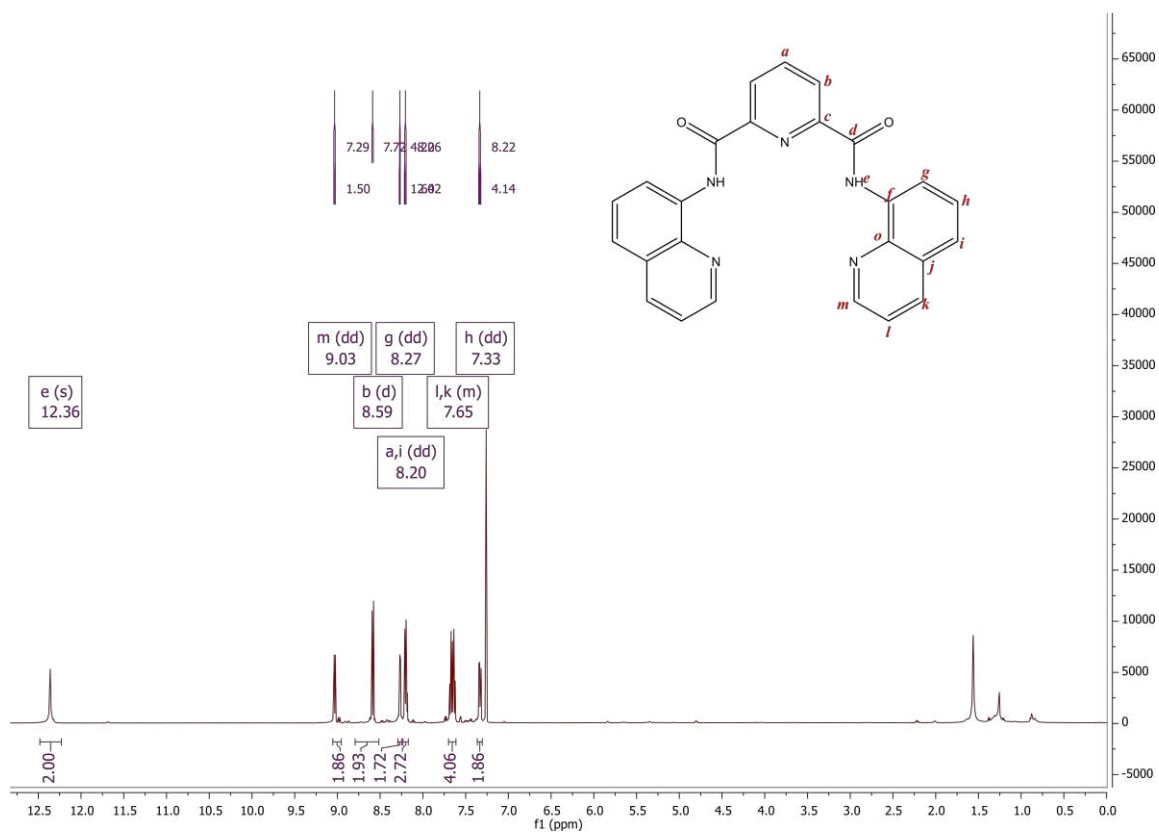
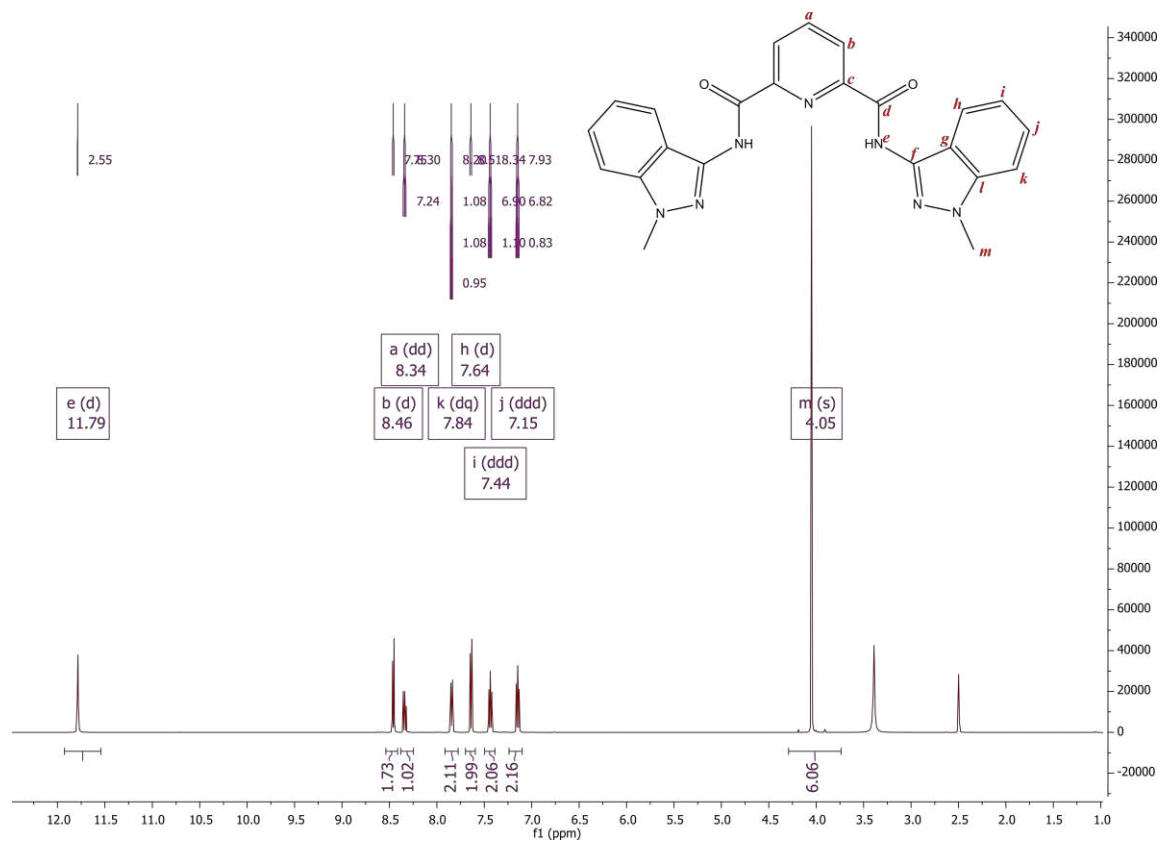


Figure S9.  $^1\text{H}$  (a) and  $^{13}\text{C}$  APT (b) NMR spectra of **1c** in  $\text{DMSO-}d_6$ .

a)



b)

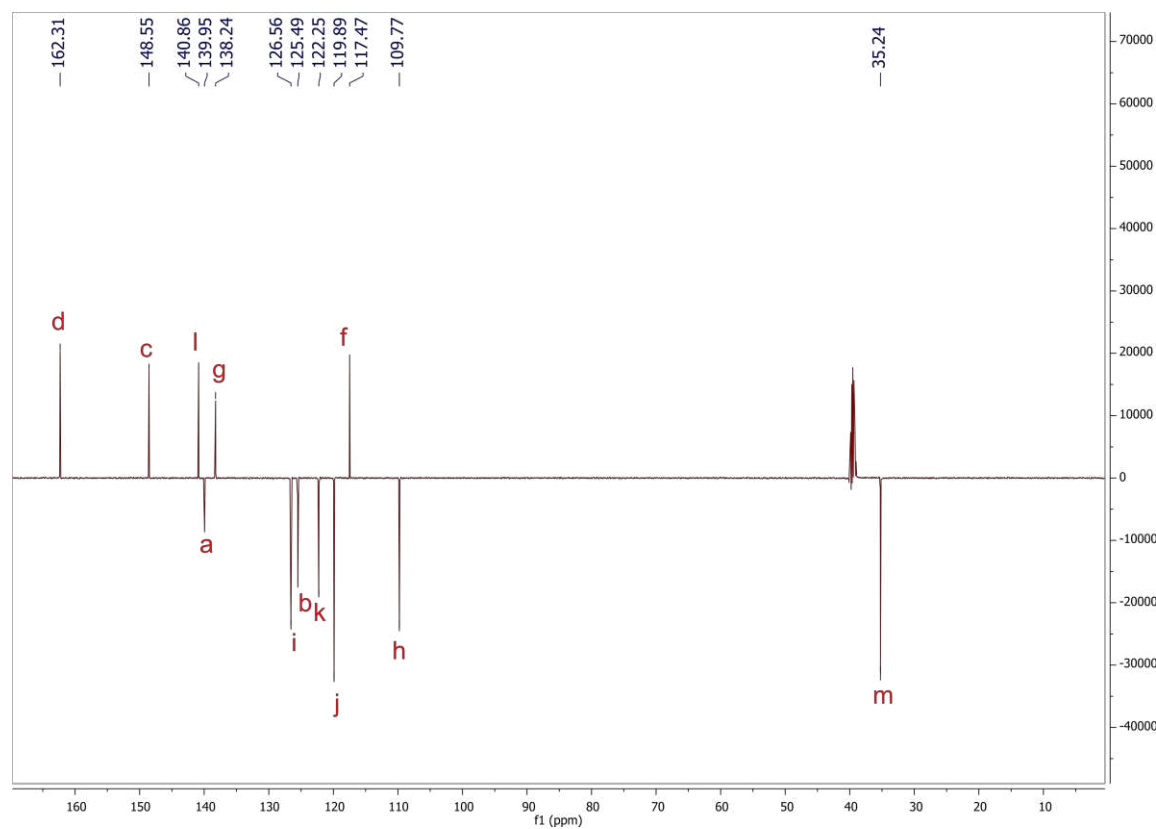


Figure S10.  $^1\text{H}$  (a) and  $^{13}\text{C}$  APT (b) NMR spectra of **1d** in  $\text{DMSO-}d_6$ .

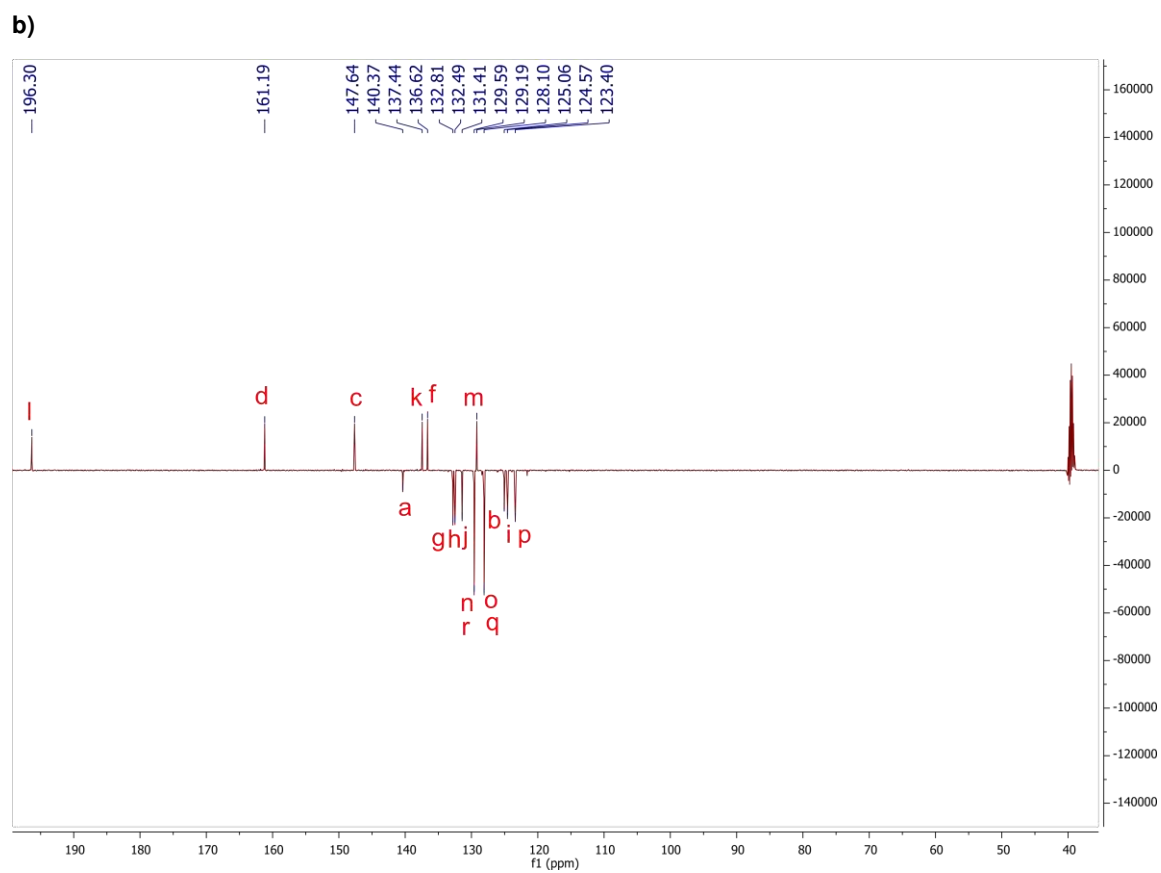
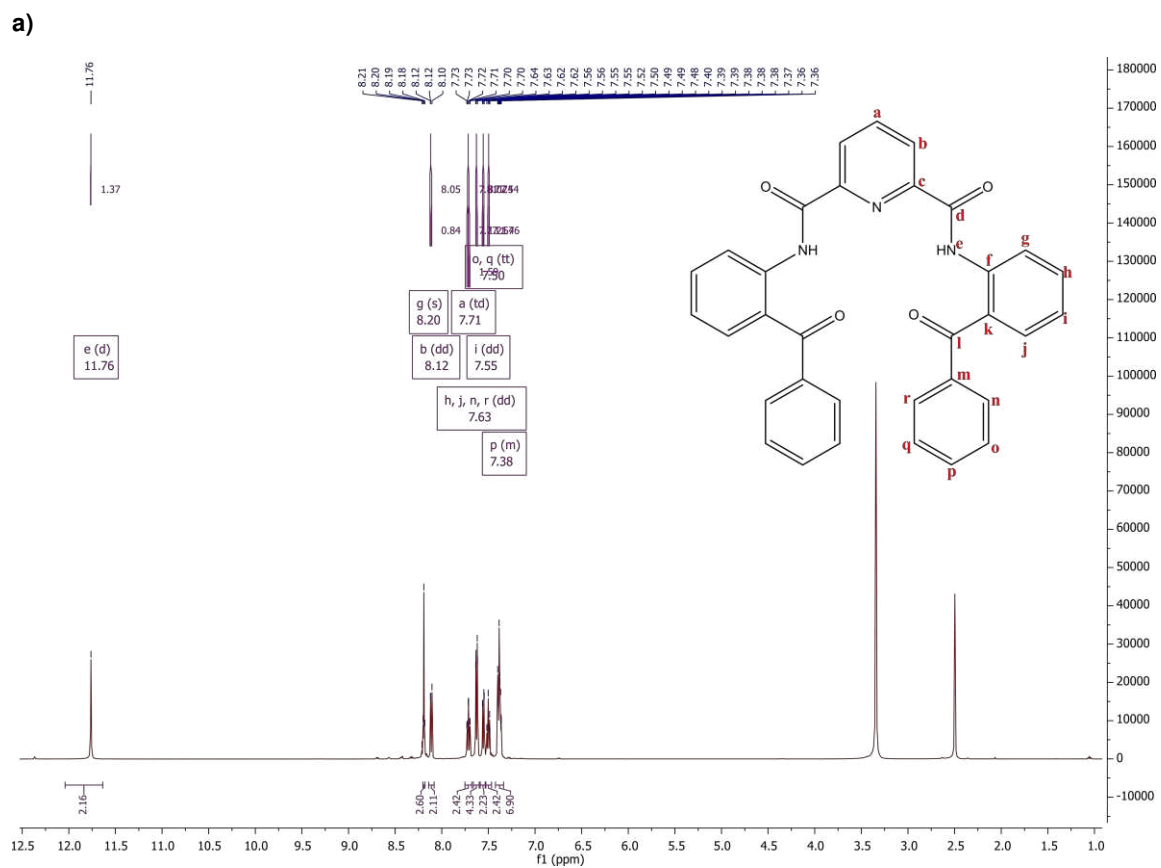
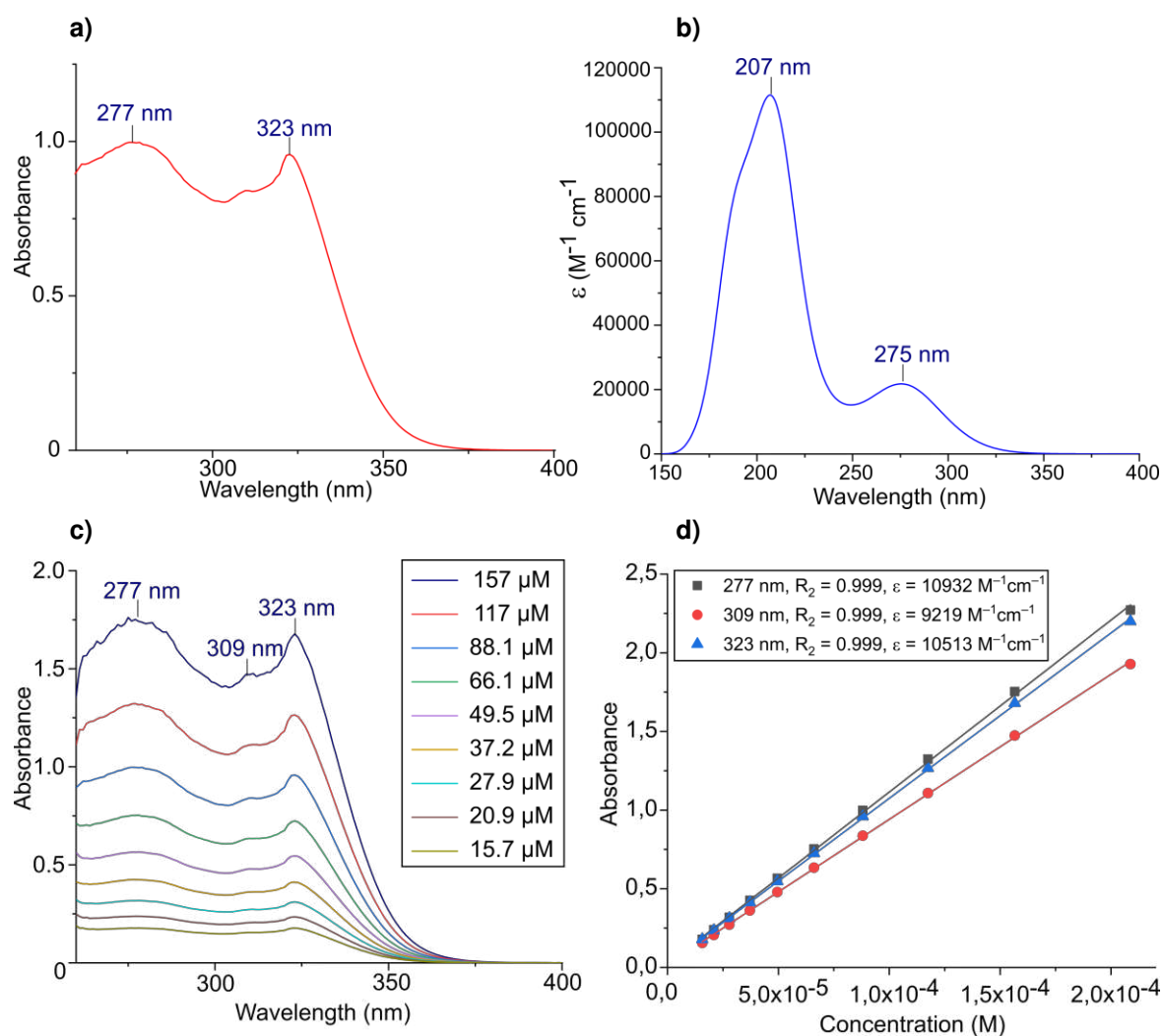


Figure S11. <sup>1</sup>H (a) and <sup>13</sup>C APT (b) NMR spectra of **1e** in MeCN-*d*<sub>3</sub>.



## UV-vis spectroscopy



**Figure S13.** (a) Experimental and (b) DFT-calculated electronic absorption spectra of **1a** in DMSO. The absorption maxima are indicated for the experimental spectrum at 277, 309 and 323 nm. The absorption envelope for the DFT-calculated spectrum is plotted with a band width of  $2200 cm^{-1}$  (full width at half maximum intensity, FWHM). (c) Absorption spectra at a concentration range between 16 and 157  $\mu M$ , and (d) Linear Beer-Lambert plot (Beer-Lambert's Law), to calculate the extinction coefficients at the  $\lambda_{max}$

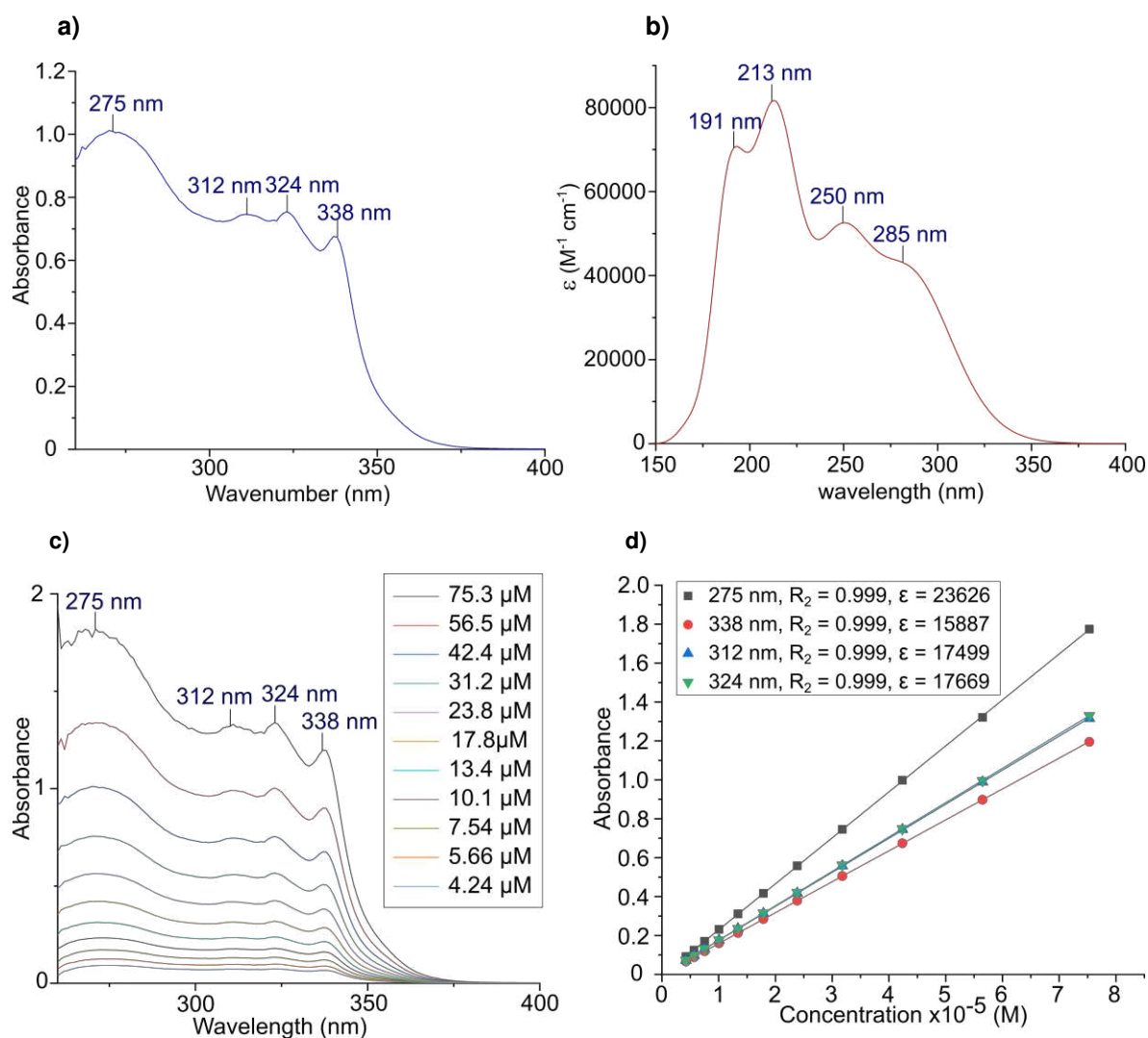


**Figure S14.** (a) Experimental and (b) DFT-calculated electronic absorption spectra of **1b** in DMSO. The absorption maxima are indicated for the experimental spectrum at 275, 312, 324 and 338 nm. The absorption envelope for the DFT-calculated spectrum is plotted with a bandwidth of  $2200\text{ cm}^{-1}$  (full width at half maximum intensity, FWHM). (c) Absorption spectra at a concentration range between 4 and 75  $\mu M$ , and (d) Linear Beer-Lambert plot (Beer-Lambert's Law), to calculate the extinction coefficients at the  $\lambda_{max}$ .

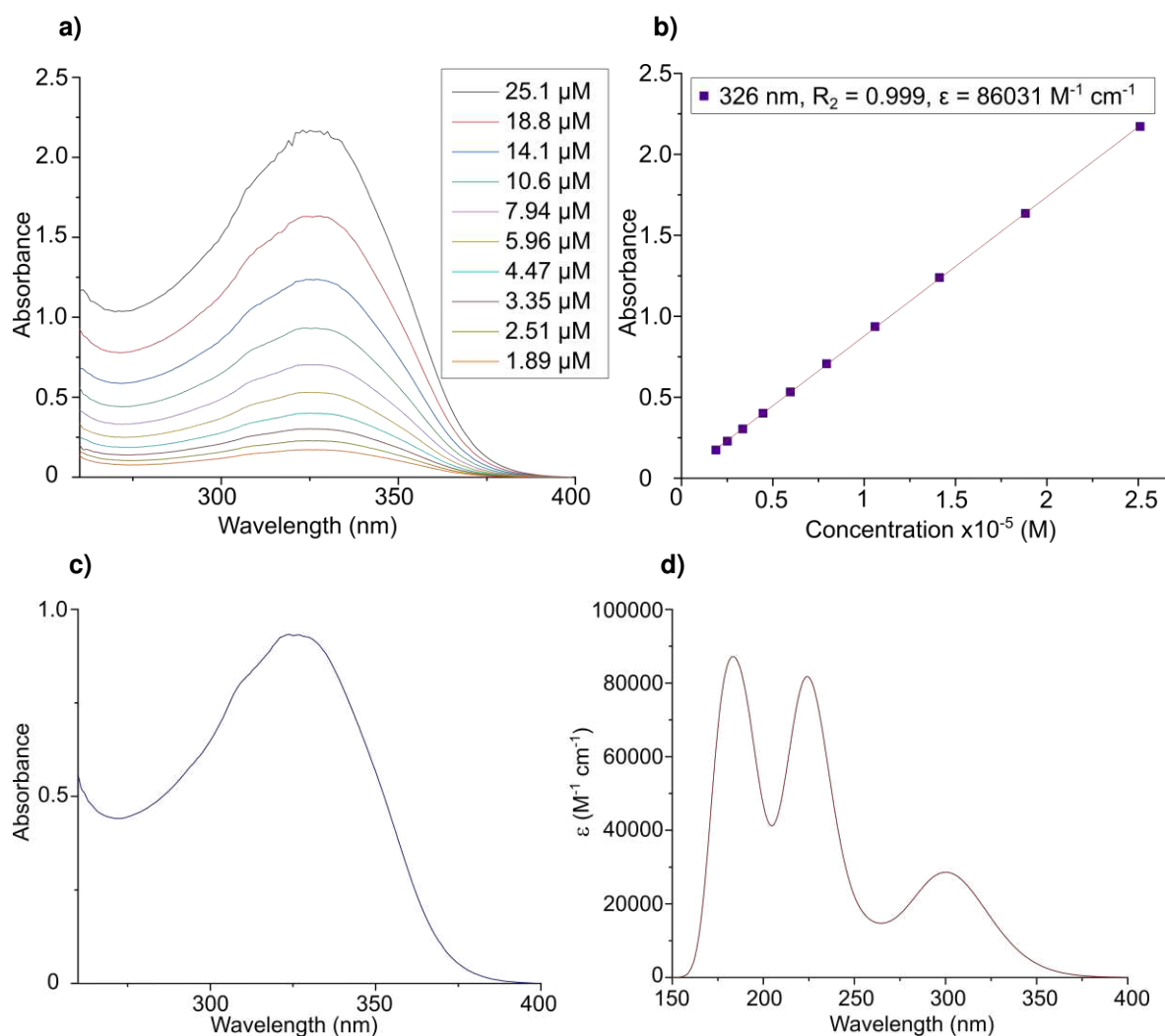


**Figure S15.** (a) Experimental and (b) DFT-calculated electronic absorption spectra of **1c** in DMSO. The absorption maxima are indicated for the experimental spectrum at 326 nm. The absorption envelope for the DFT-calculated spectrum is plotted with a bandwidth of 2200  $\text{cm}^{-1}$  (full width at half maximum intensity, FWHM). (c) Absorption spectra at a concentration range between 2 and 25  $\mu\text{M}$ , and (d) Linear Beer-Lambert plot (Beer-Lambert's Law), to calculate the extinction coefficients at the  $\lambda_{\text{max}}$ .

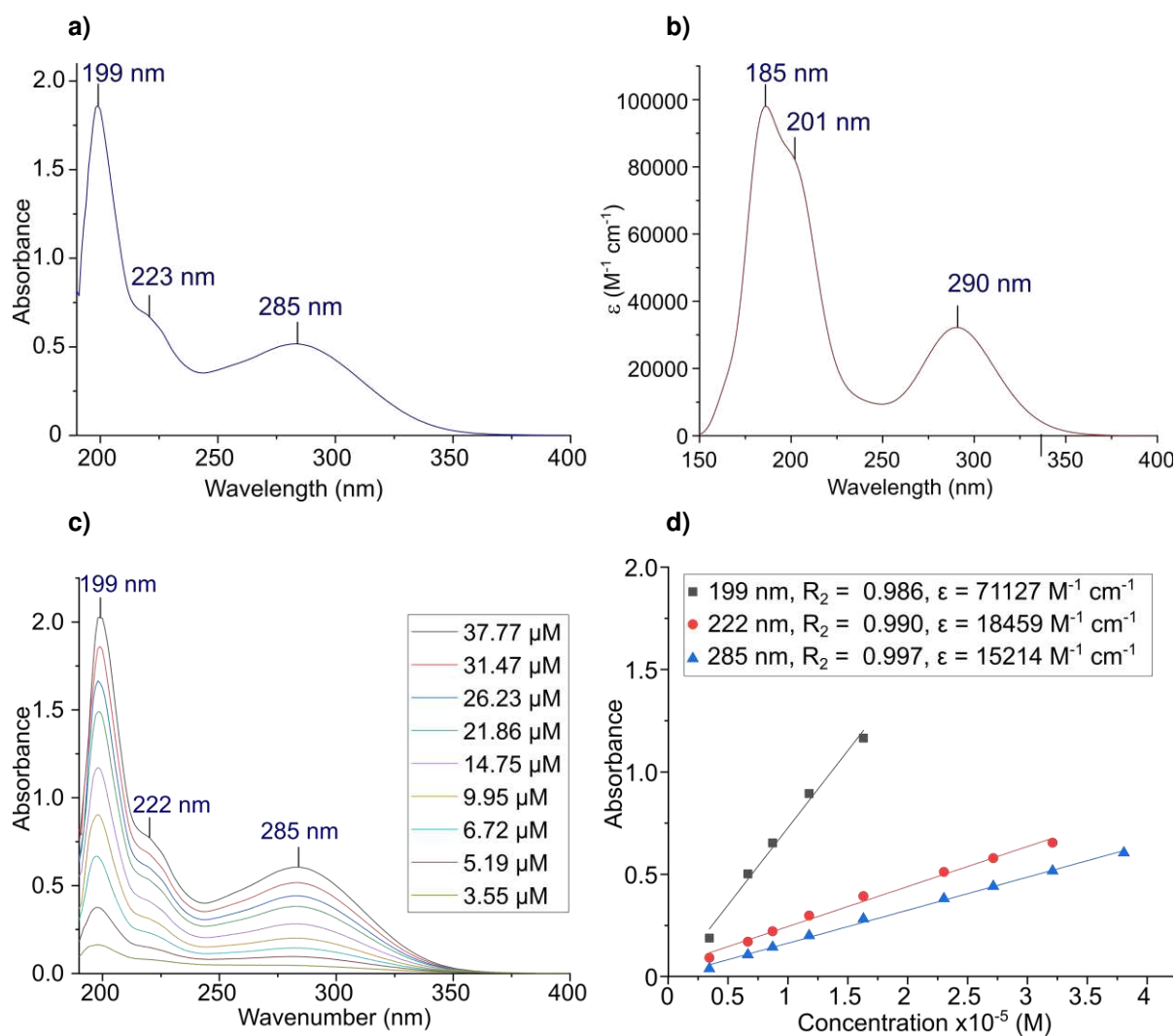


**Figure S16.** (a) Experimental and (b) DFT-calculated electronic absorption spectra of **1d** in ACN. The absorption maxima are indicated for the experimental spectrum at 199, 223, 285 nm. The absorption envelope for the DFT-calculated spectrum is plotted with a bandwidth of  $2200\text{ cm}^{-1}$  (full width at half maximum intensity, FWHM). (c) Absorption spectra at a concentration range between 4 and 38  $\mu M$ , and (d) Linear Beer-Lambert plot (Beer-Lambert's Law), to calculate the extinction coefficients at the  $\lambda_{max}$ .

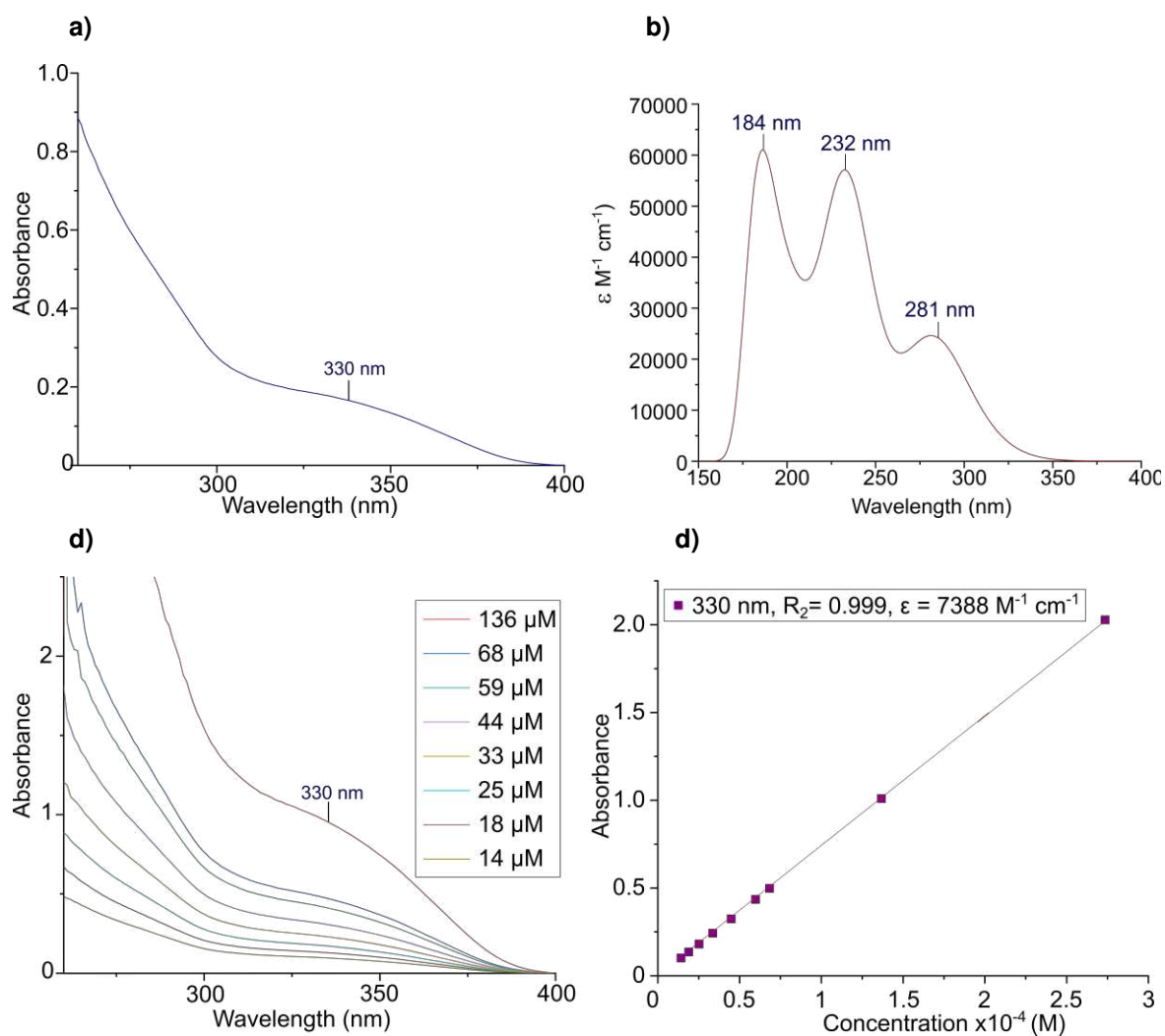


**Figure S17** (a) Experimental and (b) DFT-calculated electronic absorption spectra of **1e** in DMSO. The absorption maxima are indicated for the experimental spectrum at 330 nm. The absorption envelope for the DFT-calculated spectrum is plotted with a bandwidth of  $2200\text{ cm}^{-1}$  (full width at half maximum intensity, FWHM). (c) Absorption spectra at a concentration range between 14 and 136  $\mu M$ , and (d) Linear Beer-Lambert plot (Beer-Lambert's Law), to calculate the extinction coefficients at at the  $\lambda_{max}$ .

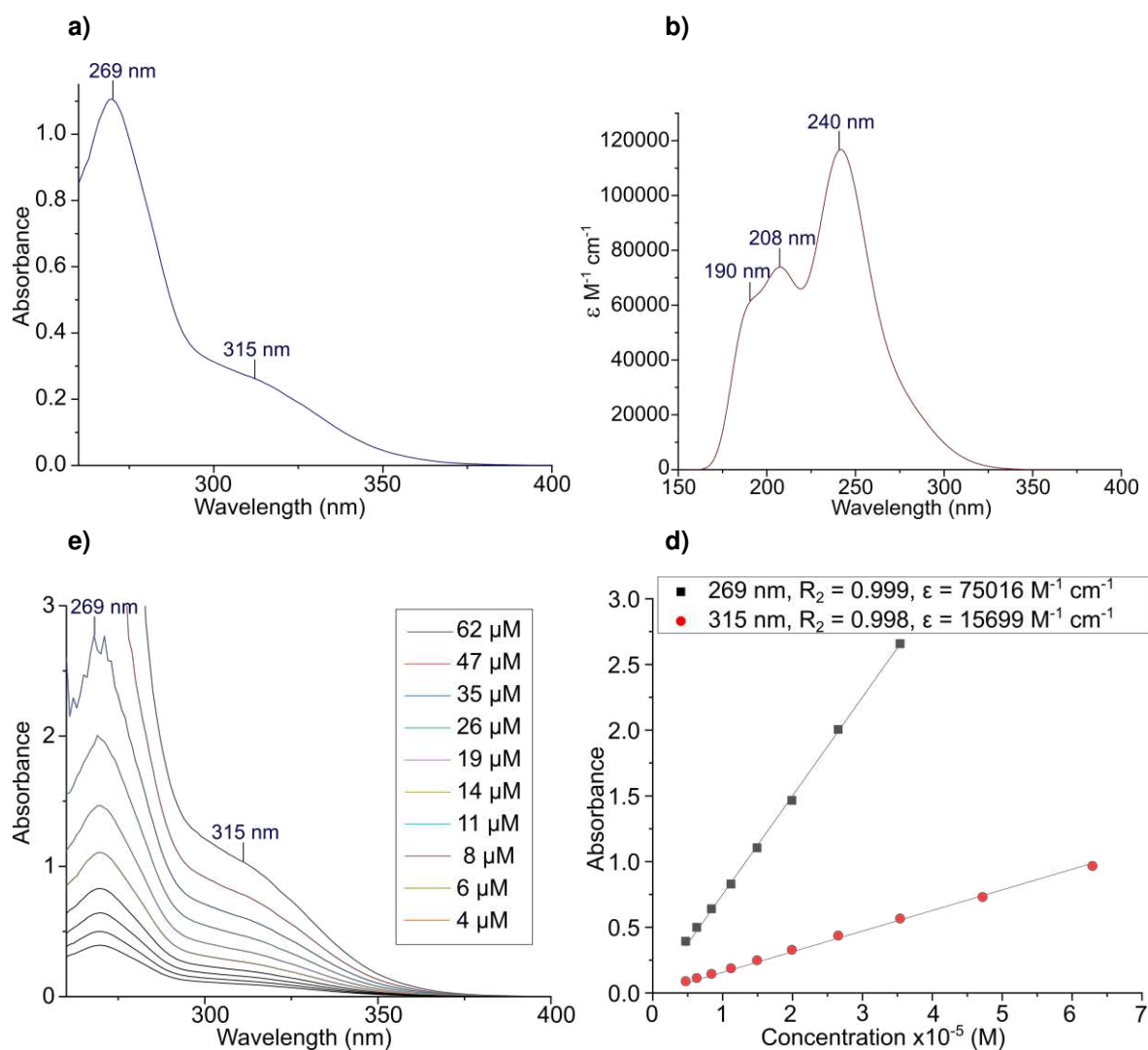


**Figure S18.** (a) Experimental and (b) DFT-calculated electronic absorption spectra of **1f** in DMSO. The absorption maxima are indicated for the experimental spectrum at 269 and 315 nm. The absorption envelope for the DFT-calculated spectrum is plotted with a bandwidth of  $2200 \text{ cm}^{-1}$  (full width at half maximum intensity, FWHM). (c) Absorption spectra at a concentration range between 4 and 62  $\mu\text{M}$ , and (d) Linear Beer-Lambert plot (Beer-Lambert's Law), to calculate the extinction coefficients at the  $\lambda_{\text{max}}$ .

**Table 1.** Calculated energies for orbital levels involved in electron transition.

	<b>1a</b>	<b>1b</b>	<b>1c</b>	<b>1d</b>	<b>1e</b>	<b>1f</b>
<b>HOMO-3</b>	-0.26131	-0.25499	-0.26722	-0.25245	-0.25803	-0.25291
<b>HOMO-2</b>	-0.26052	-0.25494	-0.26520	-0.25198	-0.25551	-0.25287
<b>HOMO-1</b>	-0.22929	-0.23079	-0.22469	-0.21323	-0.23921	-0.24191
<b>HOMO</b>	-0.22759	-0.23079	-0.22379	-0.21190	-0.23754	-0.24092
<b>LUMO</b>	-0.09851	-0.09771	-0.09416	-0.09335	-0.09723	-0.09549
<b>LUMO+1</b>	-0.09815	-0.09720	-0.09242	-0.09136	-0.09199	-0.09421
<b>LUMO+2</b>	-0.07289	-0.07690	-0.07370	-0.05764	-0.07768	-0.08091
<b>LUMO+3</b>	-0.07080	-0.07457	-0.07275	-0.05730	-0.07368	-0.07950

**Table 2.** Difference in energy between different HOMO and LUMO energy levels in eV

Energy levels		Energy difference (eV)					
		<b>1a</b>	<b>1b</b>	<b>1c</b>	<b>1d</b>	<b>1e</b>	<b>1f</b>
<b>HOMO</b>	<b>LUMO</b>	-0.12908	-0.13308	-0.12963	-0.11855	-0.14031	-0.14543
	<b>LUMO+1</b>	-0.12944	-0.13359	-0.13137	-0.12054	-0.14555	-0.14671
	<b>LUMO+2</b>	-0.1547	-0.15389	-0.15009	-0.15426	-0.15986	-0.16001
	<b>LUMO+3</b>	-0.15679	-0.15622	-0.15104	-0.1546	-0.16386	-0.16142
<b>HOMO-1</b>	<b>LUMO</b>	-0.13078	-0.13308	-0.13053	-0.11988	-0.14198	-0.14642
	<b>LUMO+1</b>	-0.13114	-0.13359	-0.13227	<b>-0.12187</b>	-0.14722	-0.1477
	<b>LUMO+2</b>	-0.1564	-0.15389	-0.15099	<b>-0.15559</b>	-0.16153	-0.161
	<b>LUMO+3</b>	-0.15849	-0.15622	-0.15194	-0.15593	-0.16553	-0.16241
<b>HOMO-2</b>	<b>LUMO</b>	-0.16201	-0.15723	-0.17104	-0.15863	-0.15828	-0.15738
	<b>LUMO+1</b>	-0.16237	-0.15774	-0.17278	-0.16062	-0.16352	-0.15866
	<b>LUMO+2</b>	-0.18763	-0.17804	-0.1915	-0.19434	-0.17783	-0.17196
	<b>LUMO+3</b>	-0.18972	-0.18037	-0.19245	-0.19468	-0.18183	-0.17337
<b>HOMO-3</b>	<b>LUMO</b>	-0.1628	-0.15728	-0.17306	-0.1591	-0.1608	-0.15742
	<b>LUMO+1</b>	-0.16316	-0.15779	-0.1748	-0.16109	-0.16604	-0.1587
	<b>LUMO+2</b>	-0.18842	-0.17809	-0.19352	-0.19481	-0.18035	-0.172
	<b>LUMO+3</b>	-0.19051	-0.18042	-0.19447	-0.19515	-0.18435	-0.17341

## Mass spectroscopy

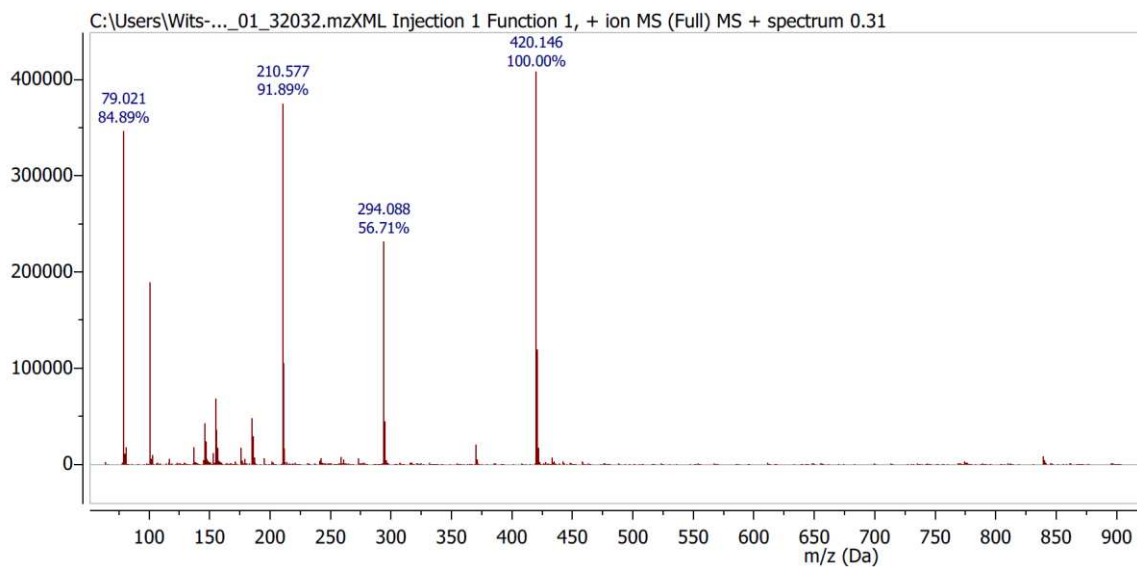


**Figure S19.** ESI-MS spectrum of **1a** for  $C_{23}H_{18}N_5O_2$   $[M+H]^+ = 420.416$ . The solid sample was dissolved in ACN (1 % DMSO) with 0.1% formic acid (v/v) and the spectrum was recorded in positive ESI mode.

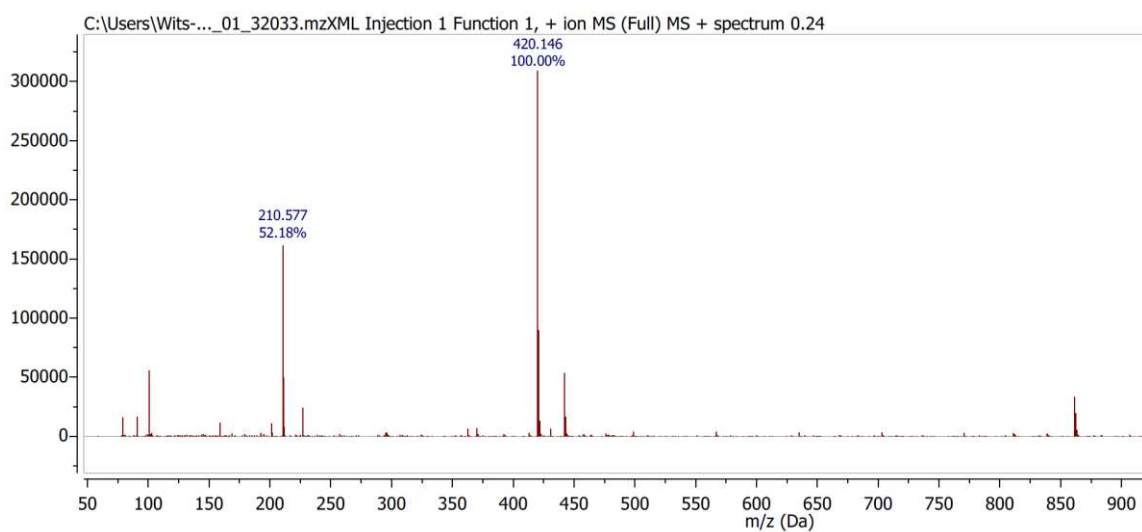


**Figure S20.** ESI-MS spectrum of **1b** for  $C_{23}H_{18}N_5O_2$   $[M+H]^+ = 420.146$ . The solid sample was dissolved in ACN (1 % DMSO) with 0.1% formic acid (v/v) and the spectrum was recorded in positive ESI mode.

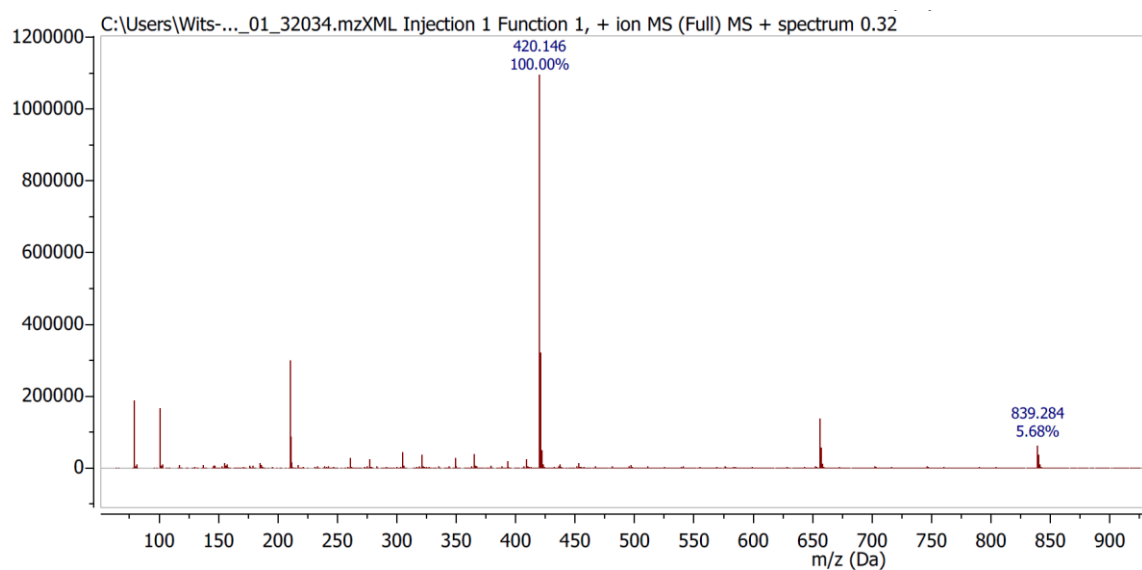


**Figure S21.** ESI-MS spectrum of **1c** for  $C_{23}H_{18}N_5O_2$   $[M+H]^+ = 420.146$ . The solid sample was dissolved in ACN (1 % DMSO) with 0.1% formic acid (v/v) and the spectrum was recorded in positive ESI mode.

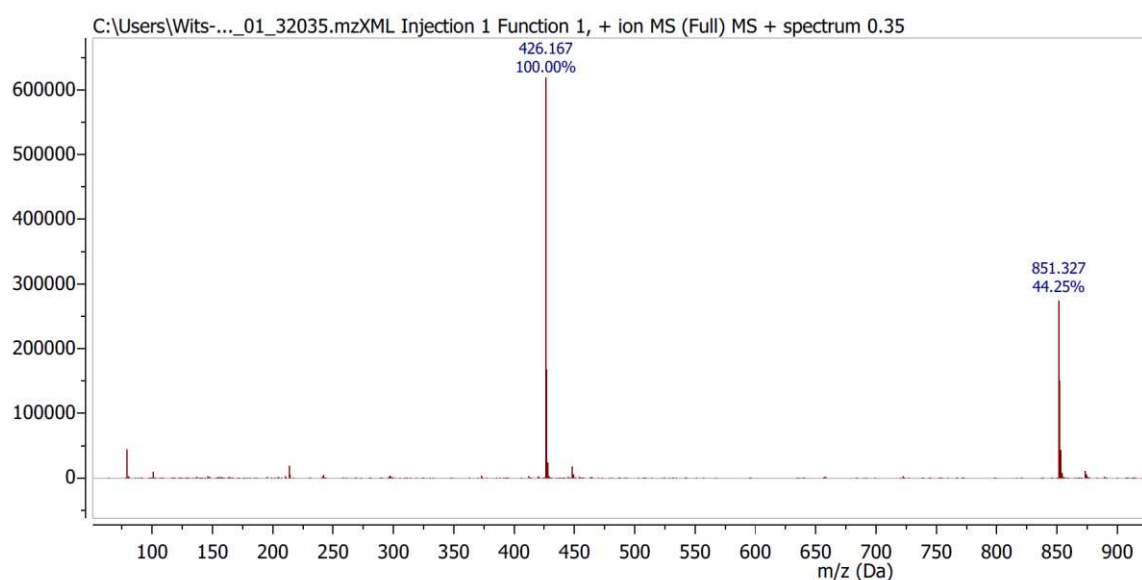


**Figure S22.** ESI-MS spectrum of **1d** for  $C_{23}H_{18}N_5O_2$   $[M+H]^+ = 420.146$ . The solid sample was dissolved in ACN with 0.1% formic acid (v/v) and the spectrum was recorded in positive ESI mode.

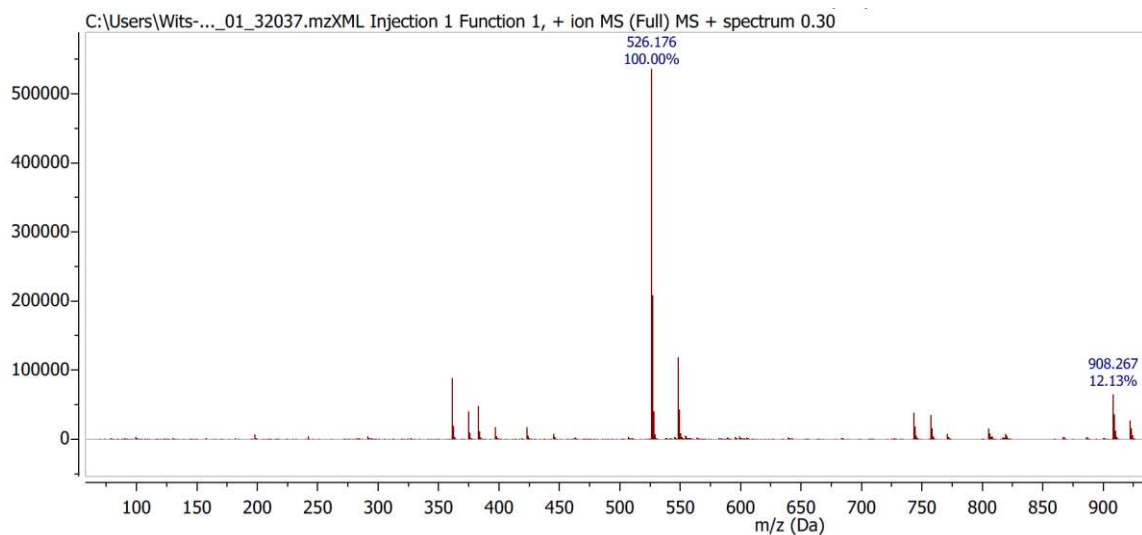


**Figure S23.** ESI-MS spectrum of **1e** for  $C_{23}H_{18}N_5O_2$   $[M+H]^+= 426.167$ . The solid sample was dissolved in ACN (1 % DMSO) with 0.1% formic acid (v/v) and the spectrum was recorded in positive ESI mode.

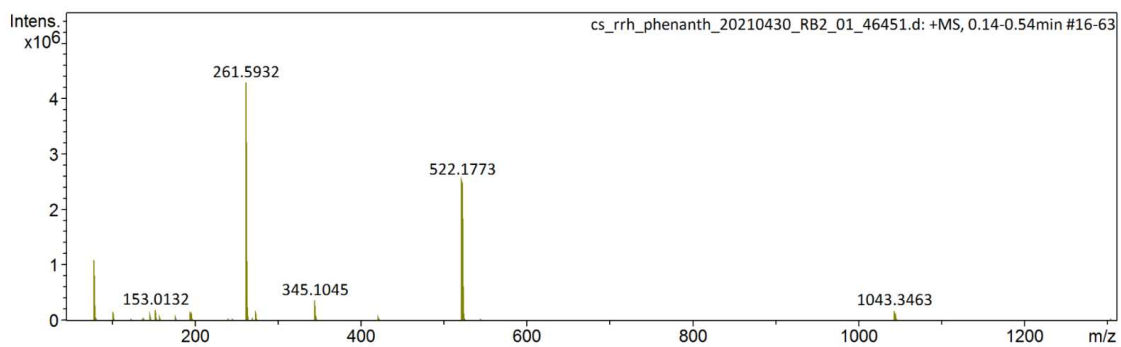


**Figure S24.** ESI-MS spectrum of **1f** for  $C_{23}H_{18}N_5O_2$   $[M+H]^+= 522.1773$ . The solid sample was dissolved in methanol with 0.1% formic acid (v/v) and the spectrum was recorded in positive ESI mode.

## Xray crystallography

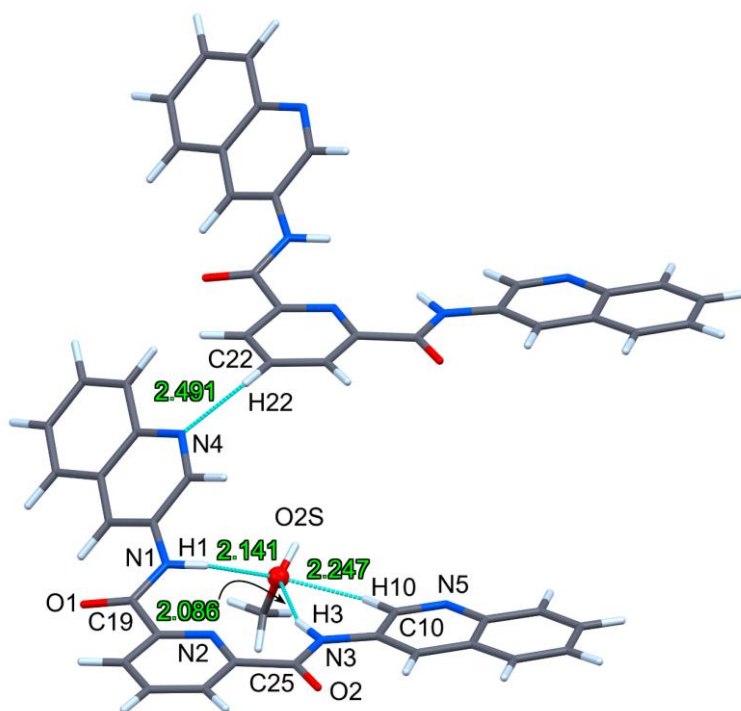


**Figure S25.** View of a pair of neighboring molecules in the crystal lattice of **1b**. The non-classical hydrogen bond C22–H22...N4 (2.491(7) Å) tips the quinoline ring out of the mean plane encompassing the central pyridine ring of the pincer, with the dihedral angle C19–N1–C2–C1 measuring 162.87(5)°. The dihedral angle for the second quinoline group (C25–N3–C11–C10, 176.31(5)°) is almost coplanar with the amide group and central pyridine ring.

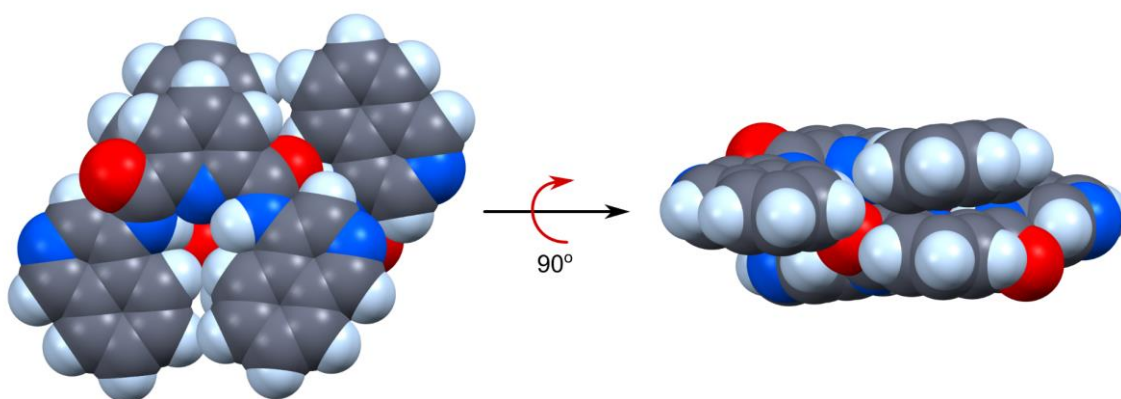


**Figure S26.** Space filling views of the hydrogen-bonded  $G_1$  symmetry dimer of structure **1a**. The diagram at the left is a view from above the dimer perpendicular to the plane of the pincer's central pyridine ring, while the diagram at the right is the same view rotated counterclockwise through 90° to highlight the out-of-plane arrangement of the two isoquinoline rings. The conformation of each monomer in the crystalline solid state is markedly different from the lowest-energy conformer in the gas phase (DFT simulation), which highlights the impact of crystal packing and dimer formation on the observed conformation.

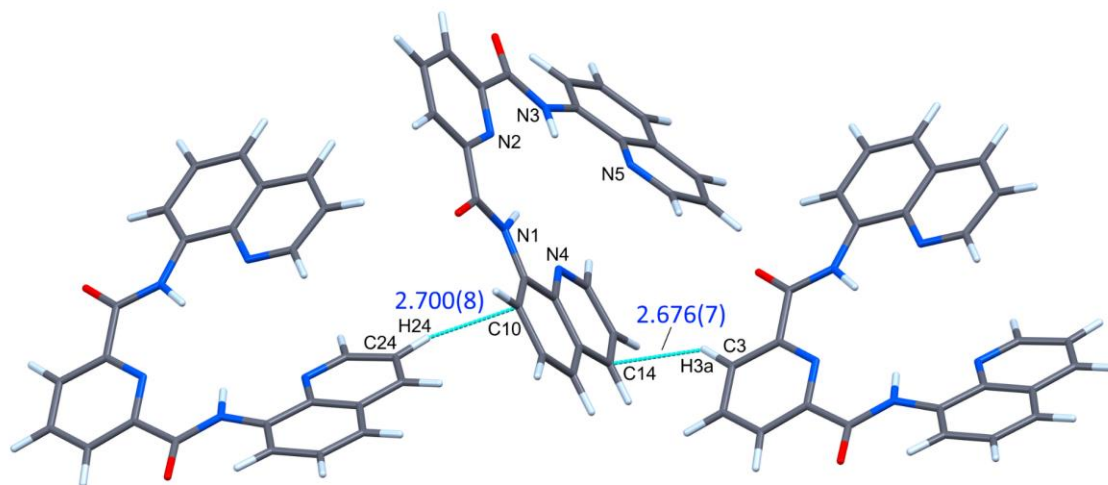


**Figure S27.** View depicting the short nonbonded interactions (blue stippled bonds) between the lower quinoline ring of **1c** and neighboring molecule heteroaromatic rings (contact distances are given in Å). The highlighted contacts constitute C–H... $\pi$  type hydrogen bonding interactions which planarise the amide group (N1) and quinoline substituent by neatly sandwiching the substituent group. The quinoline ring appended to the second amide nitrogen atom (N5) lacks short contacts involving its aryl ring carbon atoms and thus has a more canted dihedral angle relative to the plane of the central pyridine ring of the pincer.